HHS Public Access
Author manuscript
Biomaterials. Author manuscript; available in PMC 2020 August 18.

Published in final edited form as:
Biomaterials. 2020 February ; 232: 119740. doi:10.1016/j.biomaterials.2019.119740.

Microneedles for transdermal diagnostics: Recent advances and new horizons

Gui-Shi Liu[a,1], **Yifei Kong**[b,1], **Yensheng Wang**[b], **Yunhan Luo**[a], **Xudong Fan**[c], **Xi Xie**[d,*], **Bo-Ru Yang**[d,**], **Mei X. Wu**[b,***]

[a]Guangdong Provincial Key Laboratory of Optical Fiber Sensing and Communications, College of Science & Engineering, Jinan University, Guangzhou, 510632, China

[b]Wellman Center for Photomedicine, Massachusetts General Hospital, Harvard Medical School, Boston, MA, 02114, USA

[c]Department of Biomedical Engineering, University of Michigan, Ann Arbor, MI, 48109, USA

[d]State Key Laboratory of Optoelectronic Materials and Technologies, School of Electronics and Information Technology, Sun Yat-Sen University, Guangzhou, 510006, China

Abstract

Point-of-care testing (POCT), defined as the test performed at or near a patient, has been evolving into a complement to conventional laboratory diagnosis by continually providing portable, cost-effective, and easy-to-use measurement tools. Among them, microneedle-based POCT devices have gained increasing attention from researchers due to the glorious potential for detecting various analytes in a minimally invasive manner. More recently, a novel synergism between microneedle and wearable technologies is expanding their detection capabilities. Herein, we provide an overview on the progress in microneedle-based transdermal biosensors. It covers all the main aspects of the field, including design philosophy, material selection, and working mechanisms as well as the utility of the devices. We also discuss lessons from the past, challenges of the present, and visions for the future on translation of these state-of-the-art technologies from the bench to the bedside.

Keywords

Microneedle; Point-of-care; Minimally invasive; Wearable or portable biosensors; Home-based diagnosis; Continuous monitoring

[*]Corresponding author. xiexi27@mail.sysu.edu.cn (X. Xie). [**]Corresponding author. paulyang68@icloud.com (B.-R. Yang).
[***]Corresponding author. MWU5@mgh.harvard.edu (M.X. Wu).
[1]Gui-Shi Liu and Yifei Kong contributed equally.

Declaration of competing interest
The authors declare that they have no known competing financial interests or personal relationships that could have appeared to influence the work reported in this paper.

1. Introduction

Modern medicine has witnessed a continuous growth of needle-based blood collection for laboratory analyses due to high efficiency and low cost. But underneath the flourish are intractable problems: (1) reuse of un- or inappropriate-sterilized needles is common in developing countries to create a serious risk of transmitting blood-borne pathogens (*e.g.*, HIV, HBV, and HCV) [1]; (2) 3.5%−10% of the world's population expecially children holds a somewhat exaggerated form of needle phobia that may cause them to avoid seeking routine and emergency medical care [2]; (3) hypodermic needles and syringes are difficult for at-home self-administration by untrained personnel with regard to safety and waste management. Even for an easy-to-use blood glucose meter, frequent finger pricks would result in puncture-related pain and discomfort. Prausnitz et al. made remarkable progress in developing an alternative tool by shortening the needle length to around 150 μm using microfabrication technology [3]. The revolutionary design of needles, named microneedles (MNs) thereafter, guarantees not only effective drug transport across the stratum corneum (SC), but also minimal pain by without hitting nerve endings in the dermis. Since then, the research on the development of MNs has moved forward at a rapid pace [4–9].

The primary function of MNs is to gain access to biofluids beneath the skin in a nearly pain-free manner. Human skin is made up of three main layers: (1) the outermost SC layer having a thickness in the range of 10–200 μm [10]; (2) viable epidermis with interstitial fluid (ISF) beneath the SC; (3) dermis composed of blood, lymph vessels, nerve endings, and connective tissue at 300–1500 μm. A typical MN device is installed with a single needle or a needle array with a needle length of 50–2000 μm, a tip diameter of 1–100 μm, and a base width of 25–500 μm [4,6]. The MNs can be fabricated using various materials (e.g., silicon, glass, metals, and polymers) in different structures (solid, hollow, porous, coated, *etc.*) and shapes (conical, pyramidal, cylindrical, spiky, snake-fang like, *etc.*) [6]. So far, the MNs have been mainly applied to cosmetics, therapeutics, and diagnostics, among which MNs-based cosmetic treatments travel the furthest distance in practicality to be commercialized for over 10 years [8]. At present, MN-based therapeutics are in clinical trials and most research are focused on the transdermal delivery of drugs for influenza vaccination [11–15] or for treatment of diabetes mellitus [16–18], cancers [19,20], neuropathic pain [21], hair regrowth [22], and obesity [23,24].

It is not until recent years that the MNs have been used as a building block to engineer diagnostic sensors. In general, biosensors for point-of-care testing (POCT) detect medically relevant signals by analyzing external secretions (urine, saliva, sweat, and tear) or body fluids (ISF and blood) [25]. The use of external secretions are intrinsically constrained due to fewer biomarkers at lower concentrations and inaccuracy in disease screening/diagnosis [26,27]. The MNs are deemed ideal biosensing platforms since they enable extraction of or access to cutaneous body fluids in a minimally invasive way for detection of various analytes such as macromolecules, metabolites, and drugs. This new type of device greatly increases the use of ISF as a source of biomarkers for POCT. Recent studies confirmed that cutaneous ISF has similar profiles of proteins, small molecules, and RNA to blood [28–30]. Additionally, ISF contains some specific biomarkers (*e.g.*, exosomes and resident memory T cells) that are exclusive or sufficient compared to blood [30,31], which is especially true for cutaneous disorders (*e.g.*, melanoma, lupus, and psoriasis). Currently, there are two major operating modes of MN-based diagnosis: (1) extract ISF or blood that carries bioanalytes through MNs for follow-up testing; (2) adapt MNs into minuscule capturers or sensors for testing near or at the site of care. The second mode is more advantageous in terms of simplicity and speed, but of narrower applicability at the moment. No matter in which mode, the MNs are rebuilding our expectations of future medical diagnosis. Therefore, it is worthwhile to comprehensively overview the recent advances in MN-based biosensing research. Herein, the objectives of this review are to: (1) summarize the principles of MN-based detection; (2) compare the methods of MN-mediated blood/ISF extraction; (3) expound the utility of MN-based transdermal sensors for bioanalyte detection; (4) discuss the major challenges and future trends in biomedical applications of MN-based sensors.

2. Diagnosis strategies and principles

We categorize MN-based diagnosis into three modalities based on where diagnosis can be made: (1) "Off device", a MN-device is only for transdermal sampling of biofluids and the samples are transferred for central lab testing; (2) "On device", a miniaturized analyzer is integrated with a MN-device, so that sample transfer is unnecessary; (3) "On MN", every single MN mounted in a MN-device functions for *in vivo* biomarker collector or analyzer. Both "on-device" and "on-MN" modes can be adapted for use in rapid diagnostic tests at the point-of-care.

2.1. Microneedles for transdermal sampling

Biofluids (*i.e.*, ISF and blood) can be drawn out from the skin by MNs based on negative pressure, capillary force, or material absorption. Fig. 1 demonstrates the schematics of hollow (H), porous (P), and solid (S) MNs for skin biofluids sampling [32–34]. Long HMNs of > 1500 μm in length are suitable for blood sampling (see Table 1). They can draw blood from the skin using the capillary force or negative pressure. However, the capillary action is not competent for the situation where a large volume of blood is required. Therefore, a typical blood sampling device comprises a long HMN and an actuator that provides negative pressure to expedite sampling [35]. For short HMNs and PMNs (typical height < 900 μm), the capillarity of the continuous microchannels within the MN patches is preferable to extract ISF in a self-powered manner. In general, the sampling rate based on capillarity can be expedited by reducing the contact angle (θ, see Fig. 1) [36], narrowing the microchannel diameter ($2r_e$) [32], and/or inserting a wick into the HMN [37]. For SMNs, the ISF sampling can be accomplished by fluid diffusion and material absorption. The SMNs are generally made of hydrogel that is a polymeric crosslinking network containing innumerable hydrophilic groups (*e.g.*, $-NH_2$, $-OH$, and $-SO_3H$) [38]. ISF can continuously diffuse into the hydrogel SMNs, until the swelling force and the elastic network retraction force reach equilibrium. The absorbed ISF can be unloaded from the MNs by centrifugation and/or solvent extraction, while the crosslinking network of the hydrogel remains intact during manipulations [34,39].

2.2. Microneedles for transdermal detection

The “off device” diagnosis often suffers from insufficient sampling and follow-up time-consuming procedures. In contrast, both “on device” and “on MN” modes avoid the need for sample transfer, which significantly shortens the turnaround time. These two modes have four common types of designs (Fig. 2a–d): (1) attachment of a sensor to the base of an HMN patch (on device) [40–42]; (2) installment of a sensor into the lumens of HMNs (on device) [43–48]; (3) modification of SMN surface to make itself as a sensor (on MN) [49–51]; (4) metallization of SMNs as dry electrodes (on MN) [52–54].

The working principles for the four designs of MN-biosensors include colorimetry, sandwich immunoassay, enzyme-labeled electrochemical immunoassay, nucleic acid (NA) recognition, enzymatic/nonenzymic electrochemistry, and skin dry electrodes.

The sensors generally consist of a biorecognition element and an optical or electrochemical transducer. The enzyme and antibody/antigen are mostly used in the MN-based sensors for analytes recognition and capture. In a colorimetric MN sensor, the enzyme (*e.g.*, glucose oxidase) is typically used for both biorecognition and catalysis to produce hydrogen peroxide (H_2O_2) in the presence of analyte. The analyte concentration is readily estimated from the H_2O_2-induced color change of a chromogenic substrate on a paper strip (Fig. 2e) [55]. With respect to the MN immunosensors, the antibody or antigen is generally linked on the MN surface for *in vivo* protein capturing. Signal transduction relies on *in vitro* addition of secondary antibody labeled with either a fluorophore for fluorometric assay, or an enzyme for colorimetric assay, such as enzyme-linked immune sorbent assay (ELISA). When transferring ELISA to an electrode to form an electrochemical immunosensor, the analyte concentration can be quantified by monitoring the redox current between the labeled enzyme and a substrate using the electrode (Fig. 2f). Recently, peptide nucleic acids (PNAs) are immobilized on the hydrogel MNs to specifically bind complementary target DNAs via Watson-Crick base pairing (Fig. 2g) [56]. The concentration of the PNA/DNA duplex is determined using DNA intercalator either on MN or off MN after a light-triggered release process. Of note, the MNs combined with the colorimetry, ELISA, NA recognition, or electrochemical immunoassay are for a single use.

For continuous detection, MNs need to be combined with or modified into electrochemical electrodes which mainly consist of sensing materials and conductive electrodes. Most electrochemical MN sensors are enzyme-based, whereas the other sensors are enzyme-free. The majority of the enzyme-based MN sensors monitor the formation of H_2O_2 during the enzyme-catalyzed reaction of analyte, which causes a variation in the current proportional to the analyte concentration (Fig. 2h left, so called the first generation of enzymatic biosensor) [25,57]. The H_2O_2-based sensors are intrinsically influenced by the ambient concentration of dissolved oxygen in skin and require high operating voltage ranging from 0.4 to 0.7 V [44,58–60]. To avoid these issues, MNs have been combined with the second-generation sensing technique [61–63], which utilizes a redox mediator instead of H_2O_2 to shuttle electrons from the redox center of enzyme to the electrode (Fig. 2h right). For example, a low working voltage of 0.15 V was achieved for lactate detection using methylene blue as the mediator [62]. While the redox mediator-assisted MN sensors obviate the limitation of the first-generation sensing technology, they still suffer from susceptibility of enzyme activity to environmental conditions (*e.g.*, pH and temperature). In this context, non-enzymatic catalytic materials have been introduced to MN electrodes mainly for glucose monitoring [64–66]. The MN sensors utilize the non-enzymatic materials as both catalysts and mediators to interact with the analytes and to shuttle electrons between the catalysts and the electrodes (Fig. 2i). Similar detecting principle applies to the pH and nitric oxide (NO) MN sensors [50,67]. For instance, pH responsive metal oxide can directly transfer electrons from its redox reaction with H_3O^+ to electrode, which induces a potential change for pH detection [68].

Metalized MNs mounting on skin can be used as bioelectrodes for recording of biopotentials, including electrocardiography (ECG) [69], electroencephalography (EEG) [53], and electromyography (EMG) [70]. The biopotentials are monitored by at least two wet electrodes in contact with the skin; however, the traditional wet electrodes containing electrolytes give rise to a high skin impedance and unstable biopotentials during long-term diagnosis. The impedance of wet electrode-skin scheme can be modeled as a combination of an electrolyte resistance (R_e) and three impedances of the electrode to electrolyte (Z_e), the electrolyte to SC (Z_{SC}), and tissue underneath [71]. The dry MN electrode can impale the SC to directly access ISF, which circumvents the need for electrolyte and the high impedance issue arising from the SC, thus effectively eliminating R_e, Z_e, and Z_{SC} [72]. Compared to the wet electrode, the MN electrode therefore has low impedance to show superior sensitivity and long-term stability [52,53,69].

3. Biofluid extraction for off-device diagnosis

3.1. Blood extraction

Blood has long been the most important window through which clinicians can identify what is happening to a patient’s health. The dermal vasculature is located at 300–1500 μm beneath the skin surface, and therefore the HMN patch with a micro-cannula of > 1500 μm in length is frequently applied in phlebotomy [9]. Such long HMNs have been fabricated using silicon (Si) [81], polymers [82,83], and metals [84,85]. Among the structural materials, metals are mostly used due to their merits of high Young’s moduli and fracture toughness.

A typical HMN-device involves a metal micro-cannula and a vacuum-generating actuator. Actuators with different operating technologies have been developed for the HMNs, including piezoelectric [86], electrolyte-controlled [36], gel-based [87], thermopneumatic [88], and elastic actuators [89]. The elastic chamber made of polydimethylsiloxane (PDMS) is a simple and desirable actuator as negative pressure can be readily induced by elastic deformation. Jung et al. built up a PDMS chamber with an inlet and an outlet valve [35]. The two valves allowed the formation of negative pressure, rapid blood extraction, and blood transportation. The team further optimized their design with a PDMS chamber and a polymer-sealed HMN (Fig. 3a) [73]. The HMN tip was capped with polyvinyl pyrrolidone (PVP) to form a closed PDMS chamber. With high air permeability of PDMS, negative pressure was created in the closed chamber after incubation in a vacuum box, followed by depositing an airproofing parylene film to maintain the vacuum. Once the vacuumized device was pressed on skin, the PVP sealer got detached and blood was absorbed into the chamber. Animal testing confirmed a high rate of blood withdrawal (~7.8 μL s^{-1}). Inspired by the Jung et al.'s scheme, other groups reported similar HMN models without use of sealers or valves [74]. More recently, Blicharz et al. manufactured a blood collection device by enclosing a SMN array, a microchannel system, a vacuum chamber, and a reservoir in a compact chassis (Fig. 3b) [78]. The stainless steel SMNs were punched into and withdrawn from skin by a bi-stable disc spring. As a result of the vacuum actuation, ~100 μL of blood flowed into the reservoir via the microfluidic channel in 3 min. For the collection process, all a user has to do is to push the actuation button, so that special training is not mandatory.

3.2. ISF extraction

ISF is formed by blood transcapillary filtration and cleared by lymphatic vessels [90]. It is similar to blood in terms of protein diversity (93.3% in common) [28], small-molecule metabolite composition (79.3% in common) [29], and RNA profile (92.5% in common) [30]. Therefore, ISF is ideally alternative to blood for clinical diagnosis, along with advantages of good applicability in continuous monitoring due to its coagulation-free characteristic [91] and high sensitivity towards the change of local tissues. In addition, ISF extraction causes less pain due to the reduction of MN length from 1000–2000 μm to 100–800 μm (Table 1). Shorter length provides MNs with higher yield strength and shear capacity [92,93], so the short MNs for ISF sampling have greater flexibility in design and material selection.

3.2.1. Hollow microneedles—HMN holds promise not only in blood extraction, but also in ISF sampling in a painless manner. Different from extracting blood with a single needle, MN array is generally employed to withdraw enough ISF available in skin (< 1 μL mm^{-2} [94]). MN patches, with array density up to 1×10^6 needles cm^{-2}, MN height of 100–400 μm, and inner diameter of 4–100 μm, have been developed [32,88,95–97]. Short HMNs for fluid collection have been fabricated using Si [32], polymers [88], or titanium [96], but most of them resort to vacuum to extract ISF and do not demonstrate *in vivo* sampling. Si, although showing high brittleness, has been the most common single material for construction of HMNs [95,98,99], because it allows for accurate microfabrication by photolithography and endows the HMNs with the self-powered ability based on enhanced capillarity. The pioneering work by Mukerjee et al. presented a 20 × 20 array of "volcano-like" HMNs (10 μm in hole diameter) on a bulk Si wafer for *in vivo* sampling ISF [95]. It took 15–20 min to transfer ISF from human earlobe to a backside reservoir with the aid of capillary action. Strambini et al. further narrowed the inner diameter of each HMN to 4 μm and increased the density to 1×10^6 needles cm^{-2} in order to enhance capillary action, so that ISF extraction reached a flow rate of 1 μL s^{-1} (Fig. 4a) [32]. Recently, cylinder concentric substrate was used to squeeze ISF into a 5-HMN array via local mechanical pressure [30]. A large amount of ISF (up to 20 μL for 1–2 h) from human was successfully collected by the HMN-connected glass capillaries.

The high risk of hole clogging is perceived as a major concern. It has been concluded that Si HMNs with straight side-walls have a higher occlusion probability than those with tapered side-walls [40]. However, the tapered HMNs still have the clogging problem since the pore on the HMN tip tends to cut cells during the insertion. Smith et al. moved the pore to the edge of Si MN shank, forming a snake-fang-like HMN, which alleviated the plugging issue [95,97]. Another effective method is to cover the micro-channels on a Si strip with a nanoporous membrane (5 μm in thickness) [100].

3.2.2. Porous microneedles—PMNs offer a high-density network of continuous capillary channels to transfer ISF from the MN-skin interface to the base. Ceramics and metals were used to manufacture PMNs with hole diameter ranging from a few tens of nanometers to several microns [75,101,102]. The formation of porous ceramic or metal structures generally requires high sintering temperatures (*e.g.*, > 1000 °C). Therefore, porous polymers forming at much lower temperatures are a robust alternative. Porous structures for constructing MN have been generated by polymerizing acrylic monomers in the presence of porogens [76,103]. For example, by using PEG as a porogen, Liu et al. prepared a PMN from poly(glycidyl methacrylate) that was crosslinked by triethylene glycol dimethacrylate and trimethylolpropane trimethacrylate with UV irradiation [76]. The PMN patch could trigger biofluid suction by capillary action until ISF infiltrated the patch base. Like Si HMNs, the polymer PMNs are also mechanically fragile. Several teams attempted to strengthen the PMNs through reducing pore diameter and/or density; inevitably, the methods compromised sampling rate and volume [76,101]. More recently, Takeuchi et al. devised an elastic sponge-like PMN using PDMS and hyaluronic acid (HA) to conquer the fragility. The PDMS/HA MN is solid at dry state and turns into an elastic porous structure after HA dissolving, so that it can absorb fluid by manual compression and transfer the specimen to a reservoir with the help of a capillary pump (Fig. 4b) [33]. In another case, Prausnitz et al. proposed to insert porous filter papers between adjacent high-strength stainless steel SMNs [104]. However, the sandwich-structural MN can merely collect 3.3 nL ISF in 20 min. Further to this study, the same team refined their design by attaching the filter papers onto the backside of the SMN, and thus the collected volume of ISF per min reached > 2 μL [77,105].

3.2.3. Hydrogel microneedles—Hydrogel MN is a relatively new type of MNs that is hard under dry state and swells in skin without degradation. An early hydrogel MN patch was manufactured through crosslinking poly(methylvinylether/maelic acid) (PMVE/MA) with PEG [106]. The MN was first utilized for transdermal drug delivery [107], and further used to extract ISF for off-line detection of glucose, lithium, and drugs [39,80]. It required only 5-min insertion to collect sufficient ISF (0.84 μL) from excised porcine skin for analytes detection [79], but the sampling time extended to 1 h for *in vivo* experiments [39]. In order to shorten the sampling time, Chang et al. employed a super hydrating HA as a hydrogel backbone [34]. They grafted methacrylate on the HA backbones for crosslinking and then initiated free radical polymerization with UV radiation to form crosslinking network (Fig. 4c). The HA MNs successfully reduced the extraction time to 1 min. The large uptake of ISF (1.4 μL) allowed for monitoring subtle changes of ISF glucose/cholesterol levels, showing a similar trend with the real concentrations in blood. Recently, rapid ISF sampling has also been realized via a hydrogel-coated SMN patch, wherein poly(L-lactide)-made SMNs as a mechanical support pierce the skin and Ca^{2+}-alginate coating swells to extract fluids with a sampling capacity of ~6.5 μL in 2 min [56,108].

On the whole, significant advances in MN fabrication have demonstrated good feasibility in biofluid sampling over the past 5 years. Advanced MNs have been able to ultra-rapidly extract blood, such as ~100 μL in 3 min using SMNs and > 30 μL in seconds using a single HMN. As for ISF sampling, using capillary effect or material absorption, the different types of superior MNs have already shorten the extraction time to 1 min with the ascending order by sampling volume: hydrogel MN (1–3 μL) ≤ PMN (> 2 μL) < HMN (> 10 μL) (see Table 1). The sampling volume of > 1 μL can meet the need of off-line commercial analysis [34]. Sampling enough biofluids within 1 min already makes MN devices competitive to the traditional needles for blood withdrawal. Among the three kinds of MNs, hydrogel MNs and polymer PMNs are easily fabricated but need additional recovery procedures to unload ISF from the MNs, whereas the ISF extracted by HMNs can be easily transferred out of the MN lumens to the device backside by capillary action. For this reason, HMN collectors have been further developed into on-device sensors of diverse structures, while such devices based on hydrogel or porous MNs have been rarely reported. The following section will describe various integration strategies of HMN-based sensors.

4. On-device diagnosis

4.1. Single-use devices

On-device detection can be realized through affixing a specific analyzer to an HMN patch. The analyzer is typically either face-to-face mounted on the backside of the HMN patch [32,59], or just placed on the backside with connecting fluidic channels, through which biofluids are transferred to the analyzer [89]. Fig. 5a presents a typical HMN-based fluidic platform containing an immuno-modified electrode array for myoglobin/troponin detection [109]. Two syringe pumps enable fluids flow to perform an immunoassay on the antibody-decorated electrodes, followed by applying a substrate solution (3,3′5,5′-tetramethylbenzidine) to the electrodes and a chronoamperometric scan for electrochemical transduction, giving rise to current responses to both proteins in the range of 100–1000 ppb. While this kind of MN sensor minimizes an electrochemical immunoassay into a microchip platform, ISF still needs to be transferred to the microelectrodes via the complex microfluidic channels. The transfer may be limited by small volume of accessible ISF (< 1 μL mm^{-2} of skin [94]) and increases the detection time. To avoid ISF transfer and allow low-volume detection, Ranamukhaarachchi et al. integrated an immuno-modified metal HMN with an optofluidic device for vancomycin (VAN) detection (Fig. 5b) [110,111]. The lumen of the HMN was modified using the streptavidin-biotin reaction to bind a high density of peptide for VAN recognition. In this way, the microlumen, as an immunoassay reaction vessel, required only 0.6 nL ISF for analysis. Meanwhile, the high-density peptide allowed a low limit of detection (LoD) of VAN (84 nM) that was estimated from the substrate absorbance in the optofluidic channel using a photo-detector.

The HMN-fluidic biosensing platforms show proof-of-concept devices for a single use; however, the function modules of pump, buffer and agent reservoir, optical/electronic components involved in the assay are not assembled into the platforms. These components complicate the device structure and contribute to the cost of the MN sensors, which limits their application as disposable devices. One elegant design to avoid the above issues is the assembly of colorimetric strips on the backside of a HMN patch [89,95,112]. In this design, the fluid is extracted to the testing strip, where analyte is oxidized by enzyme to induce a color change of substrate (*e.g.*, 3,3′5,5′-tetramethylbenzidine). The concentration can be readily graded by naked eye or quantitatively evaluated by color analyzer. Due to simplicity of the colorimetric assay, a full-function sensing system can be easily assembled into a compact device. Fig. 5c presents such a device system including blood processing and multiple-analyte sensing [89]. It is comprised of a PDMS chamber for activation, a metal HMN for blood access, and a paper sensor for diagnostic readout. The PDMS chamber enables the uptake of 30 μL blood onto a sample pad in 30 s. The collected specimen flows through a polysulfone membrane for red blood cell filtration, after which the serum diffuses to two colorimetric reaction zones for glucose and cholesterol. The whole detection procedure is completed within 180 s. While the paper-based MN sensors represent a feasible strategy for disposable POCT diagnosis, they can only detect small-molecule analytes such as glucose and cholesterol. More studies are needed to exploit the test papers enabling protein assay for the HMN platform, so as to detect more biomarkers.

4.2. Continuous monitoring devices

Along with the evolution of disposable MN sensors, a number of research groups have exploited MNs as continuous monitoring platforms by incorporating external electrodes. They have developed a gamut of device architectures, such as defining serpentine Si nanowires on a SMN tip for pH measurement [113], hitching a nanoelectronic thread electrode to carbon/tungsten MN for long-term electrical recording [114], and mounting Ag/AgCl electrodes on a PMN patch for edema monitoring [41].

A commonly used monitoring system is structured by attaching enzymatic electrodes on the base of HMN array [40,99,116]. Fig. 6a presents a typical device for long-term glucose monitoring [59]. A three-electrode system containing a GOx-coated Pt/C working electrode was fixed on the backside reservoir of a Si HMN patch. By relieving skin response with a citrate-containing buffer preloaded in the reservoir, the prototype worked effectively for a wide concentration range (50–400 mg mL^{-1}) and a long period (up to 72 h), as validated by human testing. With similar architecture, Miller et al. extended HMN platform to K^+ sensing by potentiometry, wherein a solid-state ion-selective electrode (ISE) as transducer was connected to the HMN via fluidic microchannels (Fig. 6b) [115]. The ISE was made up of a K^+ selective membrane and a 3D porous carbon electrode fabricated by interferometric lithography. The carbon/K^+ ISE responded linearly to K^+ (10^{-5}–10^{-2} M) covering the range of normal physiological levels (3×10^{-3}–6×10^{-3} M), indicating that the device held potential in on-body K^+ monitoring. If aligned with addressable tailored electrodes, a single patch of HMN array can sense multiple physiological markers. Miller et al. developed a highly multiplexed assay of an HMN array/three tailored electrodes sensing system that could detect glucose, lactate, and pH [42].

Moving electrodes into hollow hole represents a modern strategy in HMN-sensor design. Not only it realizes highly sensitive *in situ* detection, but also prevents the electrodes from scratch damage during microneedle insertion. An early study reported palladium/aminophenol-modified carbon fibers encased inside the microlumens of a pyramidal HMN array for detecting H_2O_2 and ascorbic acid [66]. Similarly, Wang and coworkers stacked enzyme-modified SMNs on the top of pyramidal HMNs [58]. The SMNs acting as electrodes were electrodeposited with a poly(o-phenylenediamine) (PPD) layer as an entrapping matrix for glutamate oxidase and GOx, as well as an H_2O_2 permselective layer to eliminate other electroactive interferences (*e.g.*, ascorbic acid, uric acid, and cysteine) in ISF. This smart design gave rise to a good linear response to glucose (0–14 mM) or glutamate (0–140 mM). If filled with carbon paste containing metallic micro/nano-particles and oxidases, the HMNs functioned as transducers [43,117]. The renewable carbon paste electrodes supported the actual re-usage of HMNs. Moreover, the high electrocatalytic activity of metal particles towards H_2O_2 allowed for a low operating voltage, *e.g.*, −0.15 V for lactate detection with Rd particles [43]. Carbon paste was also tailored to construct a self-powered biofuel-cell (BFC) glucose sensor [117]. The sensor consisted of a carbon paste-Pt black cathode for oxygen reduction and a carbon paste bioanode containing tetrathiafulvalene (TTF) mediator and GOx. The TTF enabled shuttling electrons from the redox reaction at the enzyme to the carbon electrode [118], so that the BFC sensor continuously harvested power using glucose as a fuel. The power density of the BFC sensor have a linear response to glucose ranging from 0 to 25 mM.

While filling HMN with electrodes exhibits versatility in working electrodes and flexibility in fabrication, these devices do not incorporate counter electrode and reference electrode into a single HMN patch, so external electrodes are required to form a two/three-electrode system to conduct the electrochemical measurement. Mohan et al. presented an integrated alcohol sensor that assembled a Pt wire-based working electrode, a Pt counter electrode, and an Ag/AgCl reference electrode into a single MN patch (Fig. 6c) [44]. The Pt wire was decorated with alcohol oxidase that was sandwiched between size-exclusion PPD film and charged-exclusion Nafion film. The dual permselective layers eliminated interference of common electroactive molecules (acetaminophen, uric acid, etc.) and provided a good linear response to alcohol from 0 to 80 mM.

5. On-MN diagnosis

5.1. Microneedle immunosensors

Procedures involved in the collection/transfer of an ISF or blood sample can be omitted through transforming a SMN into an effective sensor. With the conjugation of antibody/antigen to Si SMNs, Kendall group developed a series of Si SMN-based immunosensors for capturing protein biomarkers from the skin [49,119–124]. They used a hetero-bifunctional carboxyl acid- and sulfhydryl-reactive PEG crosslinker to create linkages between capture antibodies/antigens and gold-deposited Si SMNs. After being applied to the skin for minutes to an hour, the SMNs were peeled off and incubated with dye or enzyme-labeled detection antibodies. The target biomarkers were then identified and quantified by fluorescence microscope or colorimetric enzyme-substrate reactions. This SMN/immunoassay method enabled the sensitive detection of biomarkers, including IgG antibodies [49,120,124], dengue virus NS1 protein [119], and recombinant P. falciparum (rPfHRP2) [122].

Polymers are biocompatible, inexpensive, and easy-processing materials for preparation of MN immunosensors [125–127]. Although polymer SMNs are easily fabricated using micromolding, the bald MN surface requires amine functionalization to immobilize antibodies/antigens. In one study, Yeow et al. utilized electrophilic aromatic substitution and $NaBH_4$ reduction reaction to yield an amine-enriched surface of polycarbonate (PC) SMNs, to which a hetero-bifunctional PEG derivative (*i.e.*, NHS-PEG-COOH) was linked for influenza vaccine attachment [125]. In another work, antibodies were covalently linked to hexamethylenediamine-modified polylactic acid (PLA) SMNs via homobifunctional crosslinker glutaraldehyde [126]. The former study demonstrated the sensitivity comparable to that of the gold-coated Si SMN probe for anti-influenza IgG detection, and the latter achieved a low LoD in proximity to that of ELISA for interleukins (IL)-1α testing. Moreover, the latter MN patch was functionalized in the "One Row-One Antibody (OPOA)" manner to detect IL-1α and IL-6 simultaneously. A recent work on photonic crystal (PhC) encoded SMNs took a big step forward on multiplex detection of biomarkers (Fig. 7) [127]. Differently colored PhC balls loaded with a specific type of antibody were entrapped in different PEGDA-PEG MNs. Thereupon, captured biomarkers were readily distinguished by reading the refection colors of PhC barcodes. Their concentrations were determined by measuring the fluorescence intensity. Simultaneous detection of three inflammatory cytokines (TNF-α, IL-1β, and IL-6) was performed on sepsis mice using the SMNs contained three colors of PhC barcodes. The PhC-encoded MNs demonstrate greater ease than the OPOA [126] and the LEGO-like design-knitting three smaller patches with different antibodies together into a whole patch [122], since the sensing signals from the OPOA and LEGO-like devices provide only the concentration information.

MN-based immunosensing is a promising method to identify protein markers. The capturing of proteins typically requires from 20 min to a few hours to achieve a comparable sensitivity to ELISA [119,121,128]. Such long sampling time presents a considerable hurdle to its clinical application. Efforts have been endeavored to enhance sensitivity in a short time by engineering MN surface and increasing penetrated surface area of MN. A first attempt was to minimize non-specific absorption by grafting hetero-bifunctional PEG to gold-coated MNs. The PEG could resist over 90% of passive absorption of protein [49]. On this basis, the efficiency for capturing target proteins critically relies on the immobilization strategy of detecting protein. Protein G was proposed as anchor molecules to align the detecting proteins, which improved the capture efficiency but reduced surface density of the proteins as compared to the EDC/NHS crosslinking. The detecting signals suggested that the higher density conquered the better orientation to give a higher sensitivity [119]. The sensitivity could be further improved by optimizing the EDC/NHS crosslinking for the detecting protein [120]. In addition to the surface modifications, Coffey et al. demonstrated that prolonging MN from 40 μm to 190 μm yielded a 4-fold increase in capture amount of specific IgG, enabling rapid extraction of the biomarker within 10 min [121]. Shortly thereafter, the same team increased the MN density from 20,408 MN cm^{-2} to 30,000 MN cm^{-2} and expanded the array area from 16 mm^2 to 32 mm^2 in order to enlarge the penetrated surface area, which obtained a comparable sensitivity in 30 s [123].

5.2. Microneedle electrochemical sensors

For non-metal MNs, conductive treatments are generally required to turn MN surfaces into conductive/sensing electrodes for electrical recording. Multi-walled carbon nanotube

(MWCNT) was early reported to selectively grow on a Si SMN array as a working electrode and a counter electrode for continuous glucose detection [64]. In fact, most electrical connections or electrodes were constructed by metal deposition, such as vacuum thermal/electron beam evaporation and sputter coating [53,129–131]. Two types of MNs have been developed to avoid the cumbersome vacuum deposition. One was to blend metal microparticles (palladium) into polymer (PC) solution to directly construct conductive MNs using a micro-molding process. This strategy provided the composite MNs with both catalyzing and monitoring ability towards the ferrocyanide redox [132]. The other one was adoption of hydrogel MN as the entrapping matrix of enzyme (GOx or lactose oxidase) and mediator (vinylferrocene). Caliò et al. demonstrated that the swollen hydrogel (PEGDA) MNs as conduits could couple the electrochemical current of glucose and lactic acid to the electrical contacts on the MN base [61]. Both strategies greatly simplified the preparation process for the polymer MN-based sensors, which involved only the micromolding process.

Selective and sensitive detection of biomarkers depends on redox reactions between target molecules and their enzymes. Enzymes are generally immobilized on the conductive SMNs via an electro-polymerization process, during which the enzymes are entrapped within conductive (*e.g.*, PPD and PEDOT) [58,60] or non-conductive polymers (*e.g.*, chitosan and polyphenol) [44,129]. These polymers provide a stable and biocompatible environment for enzymes, which allows the analyte of interest accessing to enzymes but restrains escape of the large enzymes. For instance, GOx within PEDOT matrix remained a good linear response to glucose between 2 and 14 mM even after the MN sensor was stored in PBS for 7 days [60]. Recently, for sensitivity enhancement, various nanomaterials including metal NPs/polymer nanofibers [133], Cu nanoflowers [134], Au-MWCNTs [62], *etc.*, have been applied to MNs as supporting structures of enzymes. The nanostructures not only provide large electroactive surface areas, but also enhance the conductivities between electrodes and enzymes. For example, Chen et al. deposited Au/Pt NPs, Pt NPs/polyaniline nanofiber, and dual permselective layers on a stainless steel MN for glucose monitoring (Fig. 8a) [133], achieving a low LoD (0.1 mM) with a broad linear range (up to 20 mM), while Bollella et al. construed a sponge-like surface using MWCNTs and polyMB for lactate detection (Fig. 8b) [62], obtaining a high sensitivity of 1473 μA cm^{-2} mM with a low LoD of 2.4 μM. However, a typical enzymatic MN sensor has to experience enzyme degradation, complicated immobilization procedure of enzyme, and oxygen limitation.

Non-enzymatic MN sensors have been exploited to overcome the critical drawbacks of the enzymatic sensors [136]. While Pt catalyst is highly active for glucose electrooxidation, smooth Pt electrodes are subject to low sensitivity, poor selectivity, and poisoning by adsorbed intermediates [137,138]. Nanoporous Pt black was electroplated at the tips of stainless steel MNs to enlarge the electroactive surface over 440 times larger than that of bare Pt electrode, favoring a high selectivity of 1.48 μA mM^{-1} cm^2 towards glucose ranging from 2 to 36 mM [65]. The Pt catalytic surface/ability was further increased by combination of Pt NPs and MWCNTs, giving rise to a higher sensitivity of 17.73 μA mM^{-1} cm^2 over the range 3–20 mM [64]. However, biofouling from the foreign body reaction accumulated on the surface of the Pt electrodes during a 7-day rabbit test, for which less and less reliable sensing was witnessed since day 5 [65]. Overcoating a biocompatible membrane would probably improve the biocompatibility of Pt NPs-based electrode.

In addition to glucose sensing, electrochemical on-MN sensors have recently emerged for monitoring NO, pH, and H_2O_2. NO has been recognized as an important messenger molecule under different physiopathological conditions (*e.g.*, a physiological indicator of colorectal cancer) [139]. Keum et al. mounted a hemin/PEDOT-modified PCL MNs on an endomicroscope to construct an instrument that enabled both real-time monitoring of NO in colonic polyps and detailed imaging of the lesions [50]. The PCL MN was exquisitely coated with hemin/PEDOT using polydopamine as a binder (Fig. 8c). The hemin offered a p-type doping effect for PEDOT via **π-π** stacking as well as high specific affinity toward NO [140]. The presence of NO reduced hemin (Fe^{3+}) to heme (Fe^{2+}), which resulted in current reduction of the PEDOT coating. Periodical response to NO with micromolar sensitivity was demonstrated by alternately applying the MNs in normal and melanoma tissues. Recent field-effect transistor sensors demonstrated that conjugation of graphene or reduced graphene oxide (rGO) with porphyrins (*e.g.*, hemin) significantly promoted selectivity and sensitivity for NO detection [140,141]. Following this design, Tang et al. synthesized iron-porphyrin functionalized graphene (FGPC) and deposited the FGPC on a PEDOT/Au NPs-coated MN [142]. The composite layer enhanced electron transfer and favored very high specific surface area for NO catalyzing [143,144], endowing the MN sensor with a LoD down to nM level.

Microneedle pH sensors were also developed by surface grafting of various pH-responsive materials [67,130,145,146]. ZnO was reported as pH sensing layer on a tungsten (W) MN because of its biocompatibility, chemical stability, and amphoteric properties [147,148]. The ZnO-W MN sensor could measure pH of 2–9 with a sensitivity of −46.35 mV pH^{-1}, and completed the pH measurement of a mouse brain or bladder within 60 s [67]. A higher sensitivity of −51.2 mV pH^{-1} was achieved using a composite of molybdenum disulfide (MoS_2) nanosheets and polyaniline (PAN) on a stainless steel MN [146]. The enhanced sensitivity attributed to high specific surface area of MoS_2 provided for H^+ sensitive PAN. The pH sensitivity could be further lifted to a super-Nernst response of 141 mV pH^{-1} by modifying a W MN with boron doped diamond (BDD), but the preparation of BBD layer involved microwave plasma-assisted chemical vapor deposition [145], leading to a complex fabrication process. Noted that the aforementioned pH responsive materials were constructed on a single metal MN without base, having disadvantages of poor reproducibility in device fabrication and varied penetration depth in measurements. Combination of a MN patch array (MPA) with pH sensing materials could avoid the issues and, moreover, provide a unique advantage in monitoring spatial distribution of pH, as demonstrated by Zuliani et al. using an iridium oxide (IrOx)-modified MPA for pH distribution mapping of an *ex vivo* rat heart [130].

The MN sensors decorated by nanomaterials exhibit superior sensing performances arising from the high specific surface area and electrocatalytic activity; however, the surface nanostructures on the MNs are susceptible to mechanical damage upon skin insertion. In a recent scheme by Xie et al., a dissolvable polymer PVP was sprayed over MN working electrodes as protective layers (Fig. 8d). The PVP layer with a thickness of 2 μm could preserve the integrity of vertical ZnO nanowires [135] or nanohybrids of rGO and Pt NPs [149] on the MN surface during insertion and dissolved in the skin in 5 min. As such, the

PVP-protected ZnO/MN sensor was three times more sensitive than that of the unprotected ZnO/MN sensor for H_2O_2 monitoring.

5.3. Microneedle biopotential recordings

Biopotentials associated with physiological processes are electrical signals generated inside the body, including, but not limited to, ECG, EEG, EMG, and electrooculogram (EOG). Such biopotentials provide biomarkers for pathological and physiological state and are often recorded using wet electrodes. However, the conventional wet electrodes for biopotential recording require tedious procedures, such as skin preparation and gel usage in order to decrease electrode-skin interface impedance [53,54]. The slow rate of gel drying is prejudicial to long-term monitoring [131,150]. Moreover, motion artifacts arising from electrode loosening and skin-potential variation (SPV) distort the signals [69,150]. Thereupon, microneedle electrode arrays (MNEAs), a novel dry electrode, were exploited to address these issues. The MNEAs penetrated through the SC to fasten the electrodes, which provided stable signals in motion states and low impedance density (*e.g.*, 7.5 kΩ cm^2@10 Hz) [53]. To further minimize motion artifacts, other types of MNEAs were developed on curved [151] or flexible substrates (*e.g.*, parylene [53], SU-8 [52], polyimide [150], and PET [70]) to accommodate body movements. Besides, Pei et al. proposed a MN-based strategy to eliminate the SPV effect. The main parts of MN electrodes were overlaid with an insulative parylene layer to avoid contact with the stratum corneum, while bare conductive MN tips exposed to the stratum germinativum [69]. This method effectively suppressed the SPV interference in a motion state. Furthermore, MN patch with high-density electrode array held a unique advantage in mapping complex muscle activity with a special pattern [54,151].

6. Conclusions, challenges, and perspectives

Over the past decades, great strides have been made in structural materials, device designs, and detection strategies to broaden the application of MN-biosensors. Based on a rich variety of detection methods, currently available MN-biosensors are capable of sensing 25 analytes (Table 2), and most are small molecules. Suitable target analytes include, but are not limited to glucose, proteins, ions, drugs, metabolites, biopotentials, and plant DNA [152]. With the rapid development, a few seconds or minutes are enough for biofluid transfer, analyte diffusion, or biorecognition (Table 1). The long collection period for proteins has been reduced to tens of seconds [123]. Recently, hydrogel-coated MNs showed the capablility of transdermal sampling of NA in 15 min and immune cells in 12 h [56,108]. The NA bound to the hydrogel hybridized with complementary target DNA, the concentration of which was determined by spectrophotometry (Fig. 9a). Aside from NA, the hydrogel can be loaded with antigen nanocapsules that solicit antigen-presenting cells (APCs) to recruit antigen-specific T cells into the hydrogel under the skin (Fig. 9b). With the remarkable past work paving the way, the MN-sensor research is on the way to a brilliant future in spite of many hurdles remaining.

Antibodies and antigens constitute one of the largest and most important classes of disease biomarkers; however, there is relatively a low equilibrium concentration for most proteins in ISF owing to their low microvascular permeability [153]. Our group found that the illumination on the skin for a few seconds with a 532-nm pulsed laser resulted in the 1000-fold concentration increase of circulating biomarkers (e.g., IgG) in the upper dermis [128,154]. When inserting MNs covalently linked with influenza antigens into the laser-treated skin, influenza antigen-specific IgG was readily detected by the MNs using mouse and pig models receiving influenza vaccines, with the sensitivity, specificity, and accuracy comparable to the immunofluorescence assay of blood samples [128]. The laser-induced capillary extravasation depends on the preferable absorbance of specific light by hemoglobin, which causes the thermal-induced dilation of capillary beneath the skin [155,156]. Likewise, Coffey et al. manually applied the local mechanical stimuli (i.e., 1–10 MPa pressure) on the skin to enhance the leakage of proteins through vessels [157]. Increasing the capillary permeability seems to be a viable strategy that enables the MNs to measure blood biomarkers in the epidermis without damage to blood vessels.

MN-based sensing for POCT is still in an immature phase. Only long-needle-based sensors (≥5 mm in length) for monitoring ISF glucose (*e.g.*, Medtronic Guardian™ Sensor and Abbott's Libre system) have already hit the store shelves [158]. In fact, more MN devices are being commercialized as a blood/ISF collector, such as TAP (Fig. 3b, Seventh Sense Biosystems Inc.) [78], HemoLink (Tasso Inc.), and an ISF absorber (Renephra Ltd.). Such devices depend on a vacuum to painlessly withdraw blood/ISF from the skin with MNs. Of note, TAP comprised of an array of 30 microneedles has received clearance from the U.S. Food and Drug Administration (FDA) in 2017 and CE Mark in 2018. So far, the FDA has just released a draft guidance to detail when a MN device should be subject to the regulation as a product, but the classification has not been made. It may take years or a decade to commercialize MN-based sensors, because it needs to be repeatedly tested for reliability, biosafety, and accessibility prior to clinical use. Design factors affecting the reliability include the length and surface uniformity of MNs and the applied mechanical stimulus [123,157]. These factors may also vary with patients regarding their age, weight, body location, and operative habit. For instance, finger press led to insufficient penetration for the MNs with ~550 μm in length or penetration failure for those with 300 μm in length [159–161]. Although an auxiliary applicator or a force sensor can ensure successful penetration [162,163], inclusion of an adequate control to standardize each assay may be more helpful for reliable results. However, whether this can address the reliability issue remains undetermined. On the other hand, both sterilization and disposal are in need of particular attention. The risk of infection is high due to the inappropriate handling and disposal of MNs [164,165]. For this reason, manufacturers are required to: (1) attach a disinfectant to MN products; (2) introduce a self-sterilizing coating onto MN surface; or (3) explore an additional enclosure for retracting or blunting MNs after use [166,167]. For a workable sensor, data collection, processing, and readout modules are indispensable. The design of MN-based biosensors that are eligible for commocialization has to take more into account, such as simple fabrication, portable size, affordable price, and adequate reliability.

In our view, research in MN-based sensors will grow rapidly in the upcoming decade. One of the key emerging trends would be the convergence of MN-biosensors, optoelectronics, and wireless communication for a comprehensive ubiquitous healthcare solution. For example, Wang et al. built up the first prototype of standalone, wearable MN-biosensor comprising HMN arrays (analyte measurement), a flexible circuit board (data processing), a

Bluetooth module (data transmission), and a battery [47]. The strip-shaped device acts as a bandage to adhere to the skin, which significantly enhances a user's comfort. Similar products came up soon on the horizon that requires the MN patches to perfectly accommodate skin deforming for a good fit [168,169]. It can be envisioned that MN-based biosensors would play a central role in a comprehensive healthcare service in the future, as depicted in Fig. 10. The wearable devices should be embedded with various smart sensors, therapeutic units, and wireless systems: (1) sensors quantify disease biomarkers and upload patients' medical records to cloud storage; (2) diagnosis is remotely performed by physicians or even artificial intelligence; (3) medical treatment decision triggers the release of preload drugs directly into the patients' bodies. Apparently, patients would benefit from the decentralization of healthcare to manage their own health at home, which may also help address the physician shortage. Overall, it is essential for academia, industry, and government to work closely so as to transform the innovations in the field into commercial products for better and more effective healthcare.

Acknowledgments

This work was supported by the Henry M. Jackson Foundation (Grant No. 309257-1.00-65282, USA) and Department of Defense/Air Force (FA9550-16-1-00173, USA) to M.X. W, National Natural Science Foundation of China (61575084 to Y. L, 61771498 to X. X), Science and Technology Planning Project of Guangdong Province for Industrial Applications (2017B090917001, China) and Science and Technology Program of Guangzhou (201803010097, China) to X. X, and the Research Grants of Sun Yat-Sen University (76120-18821104 to X. X, 76120-18843232 to B.R. Y, China).

References

[1]. Sagoe-Moses C, Pearson RD, Perry J, Jagger J, Risks to health care workers in developing countries, N. Engl. J. Med 345 (2001) 538–541. [PubMed: 11519511]

[2]. Ayala ES, Meuret AE, Ritz T, Treatments for blood-injury-injection phobia: a critical review of current evidence, J. Psychiatr. Res 43 (2009) 1235–1242. [PubMed: 19464700]

[3]. Henry S, McAllister DV, Allen MG, Prausnitz MR, Microfabricated micro-needles: a novel approach to transdermal drug delivery, J. Pharm. Sci 87 (1998) 922–925. [PubMed: 9687334]

[4]. Ventrelli L, Marsilio Strambini L, Barillaro G, Microneedles for transdermal biosensing: current picture and future direction, Adv. Healthc. Mater 4 (2015) 2606–2640. [PubMed: 26439100]

[5]. Miller PR, Narayan RJ, Polsky R, Microneedle-based sensors for medical diagnosis, J. Mater. Chem. B 4 (2016) 1379–1383. [PubMed: 32263104]

[6]. Larrañeta E, Lutton REM, Woolfson AD, Donnelly RF, Microneedle arrays as transdermal and intradermal drug delivery systems: materials science, manufacture and commercial development, Mater. Sci. Eng. R Rep 104 (2016) 1–32.

[7]. Sharma S, Hatware K, Bhadane P, Sindhikar S, Mishra DK, Recent advances in microneedle composites for biomedical applications: advanced drug delivery technologies, Mater. Sci. Eng. C 103 (2019) 109717.

[8]. Bhatnagar S, Dave K, Venuganti VVK, Microneedles in the clinic, J. Control. Release 260 (2017) 164–182. [PubMed: 28549948]

[9]. Xue P, et al., Blood sampling using microneedles as a minimally invasive platform for biomedical diagnostics, Appl. Mater. Today 13 (2018) 144–157.

[10]. Baroli B, Penetration of nanoparticles and nanomaterials in the skin: fiction or reality? J. Pharm. Sci 99 (2010) 21–50. [PubMed: 19670463]

[11]. Sullivan SP, et al., Dissolving polymer microneedle patches for influenza vaccination, Nat. Med 16 (2010) 915. [PubMed: 20639891]

[12]. Wang J, Shah D, Chen X, Anderson RR, Wu MX, A micro-sterile inflammation array as an adjuvant for influenza vaccines, Nat. Commun 5 (2014) 4447. [PubMed: 25033973]

[13]. Wang J, Li B, Wu MX, Effective and lesion-free cutaneous influenza vaccination, Proc. Natl. Acad. Sci. U.S.A 112 (2015) 5005–5010. [PubMed: 25848020]

[14]. Hirobe S, et al., Clinical study and stability assessment of a novel transcutaneous influenza vaccination using a dissolving microneedle patch, Biomaterials 57 (2015) 50–58. [PubMed: 25913250]

[15]. Bae W-G, et al., Snake fang-inspired stamping patch for transdermal delivery of liquid formulations, Sci. Transl. Med 11 (2019) eaaw3329. [PubMed: 31366579]

[16]. Ye Y, et al., Microneedles integrated with pancreatic cells and synthetic glucose-signal amplifiers for smart insulin delivery, Adv. Mater 28 (2016) 3115–3121. [PubMed: 26928976]

[17]. Wang J, et al., Core-shell microneedle gel for self-regulated insulin delivery, ACS Nano 12 (2018) 2466–2473. [PubMed: 29455516]

[18]. Lee H, et al., A graphene-based electrochemical device with thermoresponsive microneedles for diabetes monitoring and therapy, Nat. Nanotechnol 11 (2016) 566. [PubMed: 26999482]

[19]. Lan X, et al., Microneedle-mediated delivery of lipid-coated cisplatin nanoparticles for efficient and safe cancer therapy, ACS Appl. Mater. Interfaces 10 (2018) 33060–33069. [PubMed: 30204401]

[20]. Chen M-C, Lin Z-W, Ling M-H, Near-infrared light-activatable microneedle system for treating superficial tumors by combination of chemotherapy and photothermal therapy, ACS Nano 10 (2016) 93–101. [PubMed: 26592739]

[21]. Xie X, et al., Analgesic microneedle patch for neuropathic pain therapy, ACS Nano 11 (2017) 395–406. [PubMed: 28001346]

[22]. Yang G, et al., A therapeutic microneedle patch made from hair-derived keratin for promoting hair regrowth, ACS Nano 13 (2019) 4354–4360. [PubMed: 30942567]

[23]. Zhang Y, et al., Locally induced adipose tissue browning by microneedle patch for obesity treatment, ACS Nano 11 (2017) 9223–9230. [PubMed: 28914527]

[24]. Than A, et al., Transdermal delivery of anti-obesity compounds to subcutaneous adipose tissue with polymeric microneedle patches, Small Methods 1 (2017) 1700269.

[25]. Lee H, Hong YJ, Baik S, Hyeon T, Kim DH, Enzyme-based glucose sensor: from invasive to wearable device, Adv. Healthc. Mater 7 (2018) 1701150.

[26]. Nunes LAS, Mussavira S, Bindhu OS, Clinical and diagnostic utility of saliva as a non-invasive diagnostic fluid: a systematic review, Biochem. Med 25 (2015) 177.

[27]. Heikenfeld J, et al., Accessing analytes in biofluids for peripheral biochemical monitoring, Nat. Biotechnol 37 (2019) 407–419. [PubMed: 30804536]

[28]. Tran BQ, et al., Proteomic characterization of dermal interstitial fluid extracted using a novel microneedle-assisted technique, J. Proteome Res 17 (2018) 479–485. [PubMed: 29172549]

[29]. Niedzwiecki MM, et al., Human suction blister fluid composition determined using high-resolution metabolomics, Anal. Chem 90 (2018) 3786–3792. [PubMed: 29425024]

[30]. Miller PR, et al., Extraction and biomolecular analysis of dermal interstitial fluid collected with hollow microneedles, Commun. Biol 1 (2018) 173. [PubMed: 30374463]

[31]. Watanabe R, et al., Human skin is protected by four functionally and phenotypically discrete populations of resident and recirculating memory t cells, Sci. Transl. Med 7 (2015) 279ra39.

[32]. Strambini LM, et al., Self-powered microneedle-based biosensors for pain-free high-accuracy measurement of glycaemia in interstitial fluid, Biosens. Bioelectron 66 (2015) 162–168. [PubMed: 25601169]

[33]. Takeuchi K, et al., Microfluidic chip to interface porous microneedles for isf collection, Biomed, Microdevices 21 (2019) 28. [PubMed: 30847695]

[34]. Chang H, et al., A swellable microneedle patch to rapidly extract skin interstitial fluid for timely metabolic analysis, Adv. Mater 29 (2017) 1702243.

[35]. Li CG, Lee K, Lee CY, Dangol M, Jung H, A minimally invasive blood-extraction system: elastic self-recovery actuator integrated with an ultrahigh-aspect-ratio microneedle, Adv. Mater 24 (2012) 4583–4586. [PubMed: 22807158]

[36]. Chakraborty S, Tsuchiya K, Development and fluidic simulation of microneedles for painless pathological interfacing with living systems, J. Appl. Phys 103 (2008) 114701.

[37]. Li T, Barnett A, Rogers KL, Gianchandani YB, A blood sampling microsystem for pharmacokinetic applications: design, fabrication, and initial results, Lab Chip 9 (2009) 3495–3503. [PubMed: 20024028]

[38]. Ahmed EM, Hydrogel: preparation, characterization, and applications: a review, J. Adv. Res 6 (2015) 105–121. [PubMed: 25750745]

[39]. Caffarel-Salvador E, et al., Hydrogel-forming microneedle arrays allow detection of drugs and glucose in vivo: potential for use in diagnosis and therapeutic drug monitoring, PLoS One 10 (2016) e0145644.

[40]. Chua B, Desai SP, Tierney MJ, Tamada JA, Jina AN, Effect of microneedles shape on skin penetration and minimally invasive continuous glucose monitoring in vivo, Sens. Actuators A Phys 203 (2013) 373–381.

[41]. Nagamine K, Kubota J, Kai H, Ono Y, Nishizawa M, An array of porous microneedles for transdermal monitoring of intercellular swelling, Biomed. Microdevices 19 (2017) 68. [PubMed: 28776235]

[42]. Miller PR, et al., Multiplexed microneedle-based biosensor array for characterization of metabolic acidosis, Talanta 88 (2012) 739–742. [PubMed: 22265568]

[43]. Windmiller JR, et al., Microneedle array-based carbon paste amperometric sensors and biosensors, Analyst 136 (2011) 1846–1851. [PubMed: 21412519]

[44]. Mohan AMV, Windmiller JR, Mishra RK, Wang J, Continuous minimally-invasive alcohol monitoring using microneedle sensor arrays, Biosens. Bioelectron 91 (2017) 574–579. [PubMed: 28088750]

[45]. Ribet F, Stemme G, Roxhed N, Real-time intradermal continuous glucose monitoring using a minimally invasive microneedle-based system, Biomed, Microdevices 20 (2018) 101. [PubMed: 30523421]

[46]. Mishra RK, Vinu Mohan AM, Soto F, Chrostowski R, Wang J, A microneedle biosensor for minimally-invasive transdermal detection of nerve agents, Analyst 142 (2017) 918–924. [PubMed: 28220163]

[47]. Ciui B, et al., Wearable wireless tyrosinase bandage and microneedle sensors: toward melanoma screening, Adv. Healthc. Mater 7 (2018) 1701264.

[48]. Goud KY, et al., Wearable electrochemical microneedle sensor for continuous monitoring of levodopa: toward Parkinson management, ACS Sens. 4 (2019) 2196–2204. [PubMed: 31403773]

[49]. Corrie SR, et al., Surface-modified microprojection arrays for intradermal biomarker capture, with low non-specific protein binding, Lab Chip 10 (2010) 2655–2658. [PubMed: 20820632]

[50]. Keum DH, et al., Microneedle biosensor for real-time electrical detection of nitric oxide for in situ cancer diagnosis during endomicroscopy, Adv. Healthc. Mater 4 (2015) 1153–1158. [PubMed: 25728402]

[51]. Gowers SAN, et al., Development of a minimally invasive microneedle-based sensor for continuous monitoring of β-lactam antibiotic concentrations in vivo, ACS Sens. 4 (2019) 1072–1080. [PubMed: 30950598]

[52]. Stavrinidis G, et al., Su-8 microneedles based dry electrodes for electroencephalogram, Microelectron. Eng 159 (2016) 114–120.

[53]. Wang R, Jiang X, Wang W, Li Z, A microneedle electrode array on flexible substrate for long-term eeg monitoring, Sens. Actuators B Chem 244 (2017) 750–758.

[54]. Kim M, Gu G, Cha JK, Kim SD, Chung KW, Wireless semg system with a microneedle-based high-density electrode array on a flexible substrate, Sensors-Basel 18 (2018).

[55]. Blake DA, McLean NV, A colorimetric assay for the measurement of d-glucose consumption by cultured cells, Anal. Biochem 177 (1989) 156–160. [PubMed: 2742145]

[56]. Al Sulaiman D, et al., Hydrogel-coated microneedle arrays for minimally invasive sampling and sensing of specific circulating nucleic acids from skin interstitial fluid, ACS Nano 13 (2019) 9620–9628. [PubMed: 31411871]

[57]. Pappa A-M, et al., Organic electronics for point-of-care metabolite monitoring, Trends Biotechnol. 36 (2018) 45–59. [PubMed: 29196057]

[58]. Windmiller JR, et al., Bicomponent microneedle array biosensor for minimally-invasive glutamate monitoring, Electroanalysis 23 (2011) 2302–2309.

[59]. Jina A, et al., Design, development, and evaluation of a novel microneedle array-based continuous glucose monitor, J. Diabetes Sci. Technol 8 (2014) 483–487. [PubMed: 24876610]

[60]. Invernale MA, et al., Microneedle electrodes toward an amperometric glucose-sensing smart patch, Adv. Healthc. Mater 3 (2014) 338–342. [PubMed: 24039157]

[61]. Caliò A, et al., Polymeric microneedles based enzymatic electrodes for electrochemical biosensing of glucose and lactic acid, Sens. Actuators B Chem 236 (2016) 343–349.

[62]. Bollella P, Sharma S, Cass AEG, Antiochia R, Microneedle-based biosensor for minimally-invasive lactate detection, Biosens. Bioelectron 123 (2019) 152–159. [PubMed: 30177422]

[63]. Samavat S, et al., Uniform sensing layer of immiscible enzyme-mediator compounds developed via a spray aerosol mixing technique towards low cost minimally invasive microneedle continuous glucose monitoring devices, Biosens. Bioelectron 118 (2018) 224–230. [PubMed: 30092458]

[64]. Yoon Y, Lee GS, Yoo K, Lee J-B, Fabrication of a microneedle/cnt hierarchical micro/nano surface electrochemical sensor and its in-vitro glucose sensing characterization, Sensors-Basel 13 (2013) 16672–16681. [PubMed: 24304643]

[65]. Lee SJ, et al., A patch type non-enzymatic biosensor based on 3d sus micro-needle electrode array for minimally invasive continuous glucose monitoring, Sens. Actuators B Chem 222 (2016) 1144–1151.

[66]. Miller PR, et al., Integrated carbon fiber electrodes within hollow polymer microneedles for transdermal electrochemical sensing, Biomicrofluidics 5 (2011) 013415.

[67]. Mani GK, et al., Microneedle ph sensor: direct, label-free, real-time detection of cerebrospinal fluid and bladder ph, ACS Appl. Mater. Interfaces 9 (2017) 21651–21659. [PubMed: 28585801]

[68]. Qin Y, Kwon H-J, Howlader MMR, Deen MJ, Microfabricated electrochemical ph and free chlorine sensors for water quality monitoring: recent advances and research challenges, RSC Adv. 5 (2015) 69086–69109.

[69]. Pei W, et al., Skin-potential variation insensitive dry electrodes for ecg recording, IEEE Trans. Biomed. Eng 64 (2017) 463–470. [PubMed: 27164569]

[70]. Ren L, et al., Fabrication of flexible microneedle array electrodes for wearable bio-signal recording, Sensors-Basel 18 (2018) 1191.

[71]. Zhou W, et al., Characterization of impedance properties of metal dry bioelectrodes with surface microstructure arrays, Sens. Actuators A Phys 263 (2017) 252–258.

[72]. Griss P, et al., Micromachined electrodes for biopotential measurements, J. Microelectromech. Stst 10 (2001) 10–16.

[73]. Li CG, Dangol M, Lee CY, Jang M, Jung H, A self-powered one-touch blood extraction system: a novel polymer-capped hollow microneedle integrated with a pre-vacuum actuator, Lab Chip 15 (2015) 382–390. [PubMed: 25352059]

[74]. Liu L, Wang Y, Yao J, Yang C, Ding G, A minimally invasive micro sampler for quantitative sampling with an ultrahigh-aspect-ratio microneedle and a pdms actuator, Biomed. Microdevices 18 (2016) 59. [PubMed: 27372944]

[75]. Gholami S, et al., Fabrication of microporous inorganic microneedles by centrifugal casting method for transdermal extraction and delivery, Int. J. Pharm 558 (2019) 299–310. [PubMed: 30654056]

[76]. Liu L, Kai H, Nagamine K, Ogawa Y, Nishizawa M, Porous polymer micro-needles with interconnecting microchannels for rapid fluid transport, RSC Adv. 6 (2016) 48630–48635.

[77]. Kolluru C, Williams M, Chae J, Prausnitz MR, Recruitment and collection of dermal interstitial fluid using a microneedle patch, Adv. Healthc. Mater 8 (2019) 1801262.

[78]. Blicharz TM, et al., Microneedle-based device for the one-step painless collection of capillary blood samples, Nat. Biomed. Eng 2 (2018) 151–157. [PubMed: 31015714]

[79]. Romanyuk AV, et al., Collection of analytes from microneedle patches, Anal. Chem 86 (2014) 10520–10523. [PubMed: 25367229]

[80]. Eltayib E, et al., Hydrogel-forming microneedle arrays: potential for use in minimally-invasive lithium monitoring, Eur. J. Pharm. Biopharm 102 (2016) 123–131. [PubMed: 26969262]

[81]. Smart WH, Subramanian K, The use of silicon microfabrication technology in painless blood glucose monitoring, Diabetes Technol. Ther 2 (2000) 549–559. [PubMed: 11469618]

[82]. Thanh HL, et al., Optimal design of polymer-based microneedle for improved collection of whole blood from human fingers, Micro & Nano Lett. 9 (2014) 644–649.

[83]. Lee FW, Hung WH, Ma CW, Yang YJ, Polymer-based disposable microneedle array with insertion assisted by vibrating motion, Biomicrofluidics 10 (2016) 011905. [PubMed: 26858811]

[84]. Lee K, Lee HC, Lee D-S, Jung H, Drawing lithography: three-dimensional fabrication of an ultrahigh-aspect-ratio microneedle, Adv. Mater 22 (2010) 483–486. [PubMed: 20217738]

[85]. Lee D-S, Li CG, Ihm C, Jung H, A three-dimensional and bevel-angled ultrahigh aspect ratio microneedle for minimally invasive and painless blood sampling, Sens. Actuators B Chem 255 (2018) 384–390.

[86]. Tsuchiya K, Nakanishi N, Uetsuji Y, Nakamachi E, Development of blood extraction system for health monitoring system, Biomed. Microdevices 7 (2005) 347–353. [PubMed: 16404513]

[87]. Suzuki H, Tokuda T, Miyagishi T, Yoshida H, Honda N, A disposable on-line microsystem for continuous sampling and monitoring of glucose, Sens. Actuators B Chem 97 (2004) 90–97.

[88]. Jung M, An JY, Park Y, Yang S, Lee J-H, A movable polymeric microneedle array actuated by thermopneumatic force, Sens. Actuators A Phys 237 (2016) 128–135.

[89]. Li CG, et al., One-touch-activated blood multidiagnostic system using a minimally invasive hollow microneedle integrated with a paper-based sensor, Lab Chip 15 (2015) 3286–3292. [PubMed: 26190447]

[90]. Wiig H, Swartz MA, Interstitial fluid and lymph formation and transport: physiological regulation and roles in inflammation and cancer, Physiol. Rev 92 (2012) 1005–1060. [PubMed: 22811424]

[91]. Kastellorizios M, Burgess DJ, Continuous metabolic monitoring based on multi-analyte biomarkers to predict exhaustion, Sci. Rep 5 (2015) 10603. [PubMed: 26028477]

[92]. Kim K, et al., A tapered hollow metallic microneedle array using backside exposure of su-8, J. Micromech. Microeng 14 (2004) 597–603.

[93]. Park J-H, Allen MG, Prausnitz MR, Biodegradable polymer microneedles: fabrication, mechanics and transdermal drug delivery, J. Control. Release 104 (2005) 51–66. [PubMed: 15866334]

[94]. Groenendaal W, von Basum G, Schmidt KA, Hilbers PAJ, van Riel NAW, Quantifying the composition of human skin for glucose sensor development, J. Diabetes Sci. Technol 4 (2010) 1032–1040. [PubMed: 20920423]

[95]. Mukerjee EV, Collins SD, Isseroff RR, Smith RL, Microneedle array for transdermal biological fluid extraction and in situ analysis, Sens. Actuators A Phys 114 (2004) 267–275.

[96]. Kim K, Lee J-B, High aspect ratio tapered hollow metallic microneedle arrays with microfluidic interconnector, Microsyst. Technol 13 (2007) 231–235.

[97]. Smith RL, Collins SD, Duy J, Minogue TD, Silicon microneedle array for minimally invasive human health monitoring, Proceedings SPIE, 2018, p. 1049102 San Francisco, California, United States.

[98]. Stoeber B, Liepmann D, Fluid injection through out-of-plane microneedles. 1st annual international IEEE-EMBS special topic conference on microtechnologies in medicine and biology, Proceedings (Cat. No.00EX451 (2000) 224–228.

[99]. Zimmermann S, Fienbork D, Stoeber B, Flounders AW, Liepmann D, A microneedle-based glucose monitor: fabricated on a wafer-level using in-device enzyme immobilization, TRANSDUCERS ‘03. 12th International Conference on Solid-State Sensors, Actuators and Microsystems. Digest of Technical Papers (Cat. No.03TH8664), 2003, pp. 99–102.

[100]. Lee WH, et al., Microfabrication and in vivo performance of a microdialysis probe with embedded membrane, Anal. Chem 88 (2016) 1230–1237. [PubMed: 26727611]

[101]. Verhoeven M, et al., Applying ceramic nanoporous microneedle arrays as a transport interface in egg plants and an ex-vivo human skin model, Microelectron. Eng 98 (2012) 659–662.

[102]. Cahill EM, et al., Metallic microneedles with interconnected porosity: a scalable platform for biosensing and drug delivery, Acta Biomater. 80 (2018) 401–411. [PubMed: 30201432]

[103]. Humrez L, Ramos M, Al-Jumaily A, Petchu M, Ingram J, Synthesis and characterisation of porous polymer microneedles, J. Polym. Res 18 (2011) 1043–1052.

[104]. Samant PP, Prausnitz MR, Mechanisms of sampling interstitial fluid from skin using a microneedle patch, Proc. Natl. Acad. Sci. U.S.A 115 (2018) 4583. [PubMed: 29666252]

[105]. Kolluru C, et al., Monitoring drug pharmacokinetics and immunologic biomarkers in dermal interstitial fluid using a microneedle patch, Biomed. Microdevices 21 (2019) 14. [PubMed: 30725230]

[106]. Donnelly RF, et al., Hydrogel-forming microneedle arrays for enhanced transdermal drug delivery, Adv. Funct. Mater 22 (2012) 4879–4890. [PubMed: 23606824]

[107]. Donnelly RF, et al., Hydrogel-forming microneedles prepared from “super swelling” polymers combined with lyophilised wafers for transdermal drug delivery, PLoS One 9 (2014) e111547. [PubMed: 25360806]

[108]. Mandal A, et al., Cell and fluid sampling microneedle patches for monitoring skin-resident immunity, Sci. Transl. Med 10 (2018) eaar2227. [PubMed: 30429353]

[109]. Miller P, et al., Towards an integrated microneedle total analysis chip for protein detection, Electroanalysis 28 (2016) 1305–1310.

[110]. Ranamukhaarachchi SA, et al., Integrated hollow microneedle-optofluidic biosensor for therapeutic drug monitoring in sub-nanoliter volumes, Sci. Rep 6 (2016) 29075. [PubMed: 27380889]

[111]. Ranamukhaarachchi SA, Padeste C, Häfeli UO, Stoeber B, Cadarso VJ, Design considerations of a hollow microneedle-optofluidic biosensing platform incorporating enzyme-linked assays, J. Micromech. Microeng 28 (2018) 024002.

[112]. Nicholas D, et al., Rapid paper based colorimetric detection of glucose using a hollow microneedle device, Int. J. Pharm 547 (2018) 244–249. [PubMed: 29879505]

[113]. Park I, Li Z, Li X, Pisano AP, Williams RS, Towards the silicon nanowire-based sensor for intracellular biochemical detection, Biosens. Bioelectron 22 (2007) 2065–2070. [PubMed: 17056246]

[114]. Luan L, et al., Ultraflexible nanoelectronic probes form reliable, glial scar-free neural integration, Sci. Adv 3 (2017) e1601966. [PubMed: 28246640]

[115]. Miller PR, et al., Microneedle-based transdermal sensor for on-chip potentiometric determination of k+, Adv. Healthc. Mater 3 (2014) 876–881. [PubMed: 24376147]

[116]. Wang PM, Cornwell M, Prausnitz MR, Minimally invasive extraction of dermal interstitial fluid for glucose monitoring using microneedles, Diabetes Technol. Ther 7 (2005) 131–141. [PubMed: 15738711]

[117]. Valdés-Ramírez G, et al., Microneedle-based self-powered glucose sensor, Electrochem. Commun 47 (2014) 58–62.

[118]. Jia W, Valdés-Ramírez G, Bandodkar AJ, Windmiller JR, Wang J, Epidermal biofuel cells: energy harvesting from human perspiration, Angew. Chem. Int. Ed 52 (2013) 7233–7236.

[119]. Muller DA, Corrie SR, Coffey J, Young PR, Kendall MA, Surface modified microprojection arrays for the selective extraction of the dengue virus ns1 protein as a marker for disease, Anal. Chem 84 (2012) 3262–3268. [PubMed: 22424552]

[120]. Bhargav A, Muller DA, Kendall MAF, Corrie SR, Surface modifications of microprojection arrays for improved biomarker capture in the skin of live mice, ACS Appl. Mater. Interfaces 4 (2012) 2483–2489. [PubMed: 22404111]

[121]. Coffey JW, Corrie SR, Kendall MAF, Early circulating biomarker detection using a wearable microprojection array skin patch, Biomaterials 34 (2013) 9572–9583. [PubMed: 24044999]

[122]. Lee KT, et al., Capture of the circulating plasmodium falciparum biomarker hrp2 in a multiplexed format, via a wearable skin patch, Anal. Chem 86 (2014) 10474–10483. [PubMed: 25232916]

[123]. Coffey JW, Corrie SR, Kendall MAF, Rapid and selective sampling of igg from skin in less than 1 min using a high surface area wearable immunoassay patch, Biomaterials 170 (2018) 49–57. [PubMed: 29649748]

[124]. Jenkins D, Corrie S, Flaim C, Kendall M, High density and high aspect ratio solid micro-nanoprojection arrays for targeted skin vaccine delivery and specific antibody extraction, RSC Adv. 2 (2012) 3490–3495.

[125]. Yeow B, et al., Surface modification and characterization of polycarbonate microdevices for capture of circulating biomarkers, both in vitro and in vivo, Anal. Chem 85 (2013) 10196–10204. [PubMed: 24083844]

[126]. Ng KW, Lau WM, Williams AC, Towards pain-free diagnosis of skin diseases through multiplexed microneedles: biomarker extraction and detection using a highly sensitive blotting method, Drug Deliv. Transl. Res 5 (2015) 387–396. [PubMed: 25939431]

[127]. Zhang X, Chen G, Bian F, Cai L, Zhao Y, Encoded microneedle arrays for detection of skin interstitial fluid biomarkers, Adv. Mater 0 (2019) 1902825.

[128]. Li B, Wang J, Yang SY, Zhou C, Wu MX, Sample-free quantification of blood biomarkers via laser-treated skin, Biomaterials 59 (2015) 30–38. [PubMed: 25950985]

[129]. Sharma S, Saeed A, Johnson C, Gadegaard N, Cass AEG, Rapid, low cost prototyping of transdermal devices for personal healthcare monitoring, Sens. Biosensing Res 13 (2017) 104–108. [PubMed: 28424755]

[130]. Zuliani C, et al., An array of individually addressable micro-needles for mapping ph distributions, Analyst 141 (2016) 4659–4666. [PubMed: 27243147]

[131]. Chen K, et al., Fabrication of micro-needle electrodes for bio-signal recording by a magnetization-induced self-assembly method, Sensors (Basel) 16 (2016) 1533.

[132]. McConville A, Davis J, Transdermal microneedle sensor arrays based on palladium: polymer composites, Electrochem. Commun 72 (2016) 162–165.

[133]. Chen D, Wang C, Chen W, Chen Y, Zhang JXJ, Pvdf-nafion nanomembranes coated microneedles for in vivo transcutaneous implantable glucose sensing, Biosens. Bioelectron 74 (2015) 1047–1052. [PubMed: 26276540]

[134]. Fang Y, et al., Development of cu nanoflowers modified the flexible needle-type microelectrode and its application in continuous monitoring glucose in vivo, Biosens, Bioelectron 110 (2018) 44–51. [PubMed: 29587193]

[135]. Liu F, et al., Protection of nanostructures-integrated microneedle biosensor using dissolvable polymer coating, ACS Appl. Mater. Interfaces 11 (2019) 4809–4819. [PubMed: 30628778]

[136]. Chinnadayyala SR, Park I, Cho S, Nonenzymatic determination of glucose at near neutral ph values based on the use of nafion and platinum black coated microneedle electrode array, Microchim. Acta 185 (2018) 250.

[137]. Bae IT, Yeager E, Xing X, Liu CC, In situ infrared studies of glucose oxidation on platinum in an alkaline medium, J. Electroanal. Chem. Interfacial Electrochem 309 (1991) 131–145.

[138]. Park S, Chung TD, Kim HC, Nonenzymatic glucose detection using mesoporous platinum, Anal. Chem 75 (2003) 3046–3049. [PubMed: 12964749]

[139]. Chowdhury R, et al., Nitric oxide produced endogenously is responsible for hypoxia-induced hif-1α stabilization in colon carcinoma cells, Chem. Res. Toxicol 25 (2012) 2194–2202. [PubMed: 22971010]

[140]. Jiang S, et al., Real-time electrical detection of nitric oxide in biological systems with sub-nanomolar sensitivity, Nat. Commun 4 (2013) 2225. [PubMed: 23887829]

[141]. Xie H, et al., Real-time monitoring of nitric oxide at single-cell level with porphyrin-functionalized graphene field-effect transistor biosensor, Anal. Chem 88 (2016) 11115–11122. [PubMed: 27779853]

[142]. Tang L, et al., A sensitive acupuncture needle microsensor for real-time monitoring of nitric oxide in acupoints of rats, Sci. Rep 7 (2017) 6446. [PubMed: 28744003]

[143]. Wang W, Xu G, Cui XT, Sheng G, Luo X, Enhanced catalytic and dopamine sensing properties of electrochemically reduced conducting polymer nanocomposite doped with pure graphene oxide, Biosens. Bioelectron 58 (2014) 153–156. [PubMed: 24632460]

[144]. Park H, Brown PR, Bulović V, Kong J, Graphene as transparent conducting electrodes in organic photovoltaics: studies in graphene morphology, hole transporting layers, and counter electrodes, Nano Lett. 12 (2012) 133–140. [PubMed: 22107487]

[145]. Fierro S, Seishima R, Nagano O, Saya H, Einaga Y, In vivo ph monitoring using boron doped diamond microelectrode and silver needles: application to stomach disorder diagnosis, Sci. Rep 3 (2013) 3257. [PubMed: 24247214]

[146]. Zhou J-X, et al., Monitoring of ph changes in a live rat brain with mos2/pan functionalized microneedles, Analyst 143 (2018) 4469–4475. [PubMed: 30151517]

[147]. Al-Hilli SM, Al-Mofarji RT, Willander M, Zinc oxide nanorod for intracellular ph sensing, Appl. Phys. Lett 89 (2006) 173119.

[148]. Al-Hilli SM, Willander M, Öst A, Strålfors P, Zno nanorods as an intracellular sensor for ph measurements, J. Appl. Phys 102 (2007) 084304.

[149]. Jin Q, et al., Reduced graphene oxide nanohybrid-assembled microneedles as mini-invasive electrodes for real-time transdermal biosensing, Small 15 (2019) 1804298.

[150]. Ren L, et al., Flexible microneedle array electrode using magnetorheological drawing lithography for bio-signal monitoring, Sens. Actuators A Phys 268 (2017) 38–45.

[151]. Kim M, Kim T, Kim SD, Chung KW, Curved microneedle array-based semg electrode for robust long-term measurements and high selectivity, Sensors-Basel 15 (2015).

[152]. Paul R, et al., Extraction of plant DNA by microneedle patch for rapid detection of plant diseases, ACS Nano 13 (2019) 6540–6549. [PubMed: 31179687]

[153]. Fogh-Andersen N, Altura BM, Altura BT, Siggaard-Andersen O, Composition of interstitial fluid, Clin. Chem 41 (1995) 1522. [PubMed: 7586528]

[154]. Wu JH, Li B, Wu MX, Laser-induced capillary leakage for blood biomarker detection and vaccine delivery via the skin, J. Biophot 9 (2016) 676–682.

[155]. Zijlstra WG, Buursma A, Spectrophotometry of hemoglobin: absorption spectra of bovine oxyhemoglobin, deoxyhemoglobin, carboxyhemoglobin, and methemoglobin, Comp. Biochem. Physiol. B Biochem. Mol. Biol 118 (1997) 743–749.

[156]. Anderson RR, Parrish JA, Selective photothermolysis: precise microsurgery by selective absorption of pulsed radiation, Science 220 (1983) 524. [PubMed: 6836297]

[157]. Coffey JW, Meliga SC, Corrie SR, Kendall MAF, Dynamic application of microprojection arrays to skin induces circulating protein extravasation for enhanced biomarker capture and detection, Biomaterials 84 (2016) 130–143. [PubMed: 26826791]

[158]. Girardin CM, Huot C, Gonthier M, Delvin E, Continuous glucose monitoring: a review of biochemical perspectives and clinical use in type 1 diabetes, Clin. Biochem 42 (2009) 136–142. [PubMed: 18951887]

[159]. Martanto W, Moore JS, Couse T, Prausnitz MR, Mechanism of fluid infusion during microneedle insertion and retraction, J. Control. Release 112 (2006) 357–361. [PubMed: 16626836]

[160]. Verbaan FJ, et al., Assembled microneedle arrays enhance the transport of compounds varying over a large range of molecular weight across human dermatomed skin, J. Control. Release 117 (2007) 238–245. [PubMed: 17196697]

[161]. Verbaan FJ, et al., Improved piercing of microneedle arrays in dermatomed human skin by an impact insertion method, J. Control. Release 128 (2008) 80–88. [PubMed: 18394741]

[162]. Quinn HL, Hughes CM, Donnelly RF, In vivo and qualitative studies investigating the translational potential of microneedles for use in the older population, Drug Deliv. Transl. Res 8 (2018) 307–316. [PubMed: 28508376]

[163]. Norman JJ, et al., Microneedle patches: usability and acceptability for self-vaccination against influenza, Vaccine 32 (2014) 1856–1862. [PubMed: 24530146]

[164]. Donnelly RF, et al., Microneedle arrays allow lower microbial penetration than hypodermic needles in vitro, Pharma Res. 26 (2009) 2513–2522.

[165]. McConville A, Hegarty C, Davis J, Mini-review: assessing the potential impact of microneedle technologies on home healthcare applications, Medicines 5 (2018) 50.

[166]. Donnelly RF, et al., Hydrogel-forming microneedle arrays exhibit antimicrobial properties: potential for enhanced patient safety, Int. J. Pharm 451 (2013) 76–91. [PubMed: 23644043]

[167]. González García LE, et al., Self-sterilizing antibacterial silver-loaded microneedles, Chem. Commun 55 (2019) 171–174.

[168]. Xu S, et al., Soft microfluidic assemblies of sensors, circuits, and radios for the skin, Science 344 (2014) 70–74. [PubMed: 24700852]

[169]. Kim D-H, et al., Epidermal electronics, Science 333 (2011) 838–843. [PubMed: 21836009]

[170]. Parrilla M, et al., Wearable all-solid-state potentiometric microneedle patch for intradermal potassium detection, Anal. Chem 91 (2019) 1578–1586. [PubMed: 30543102]

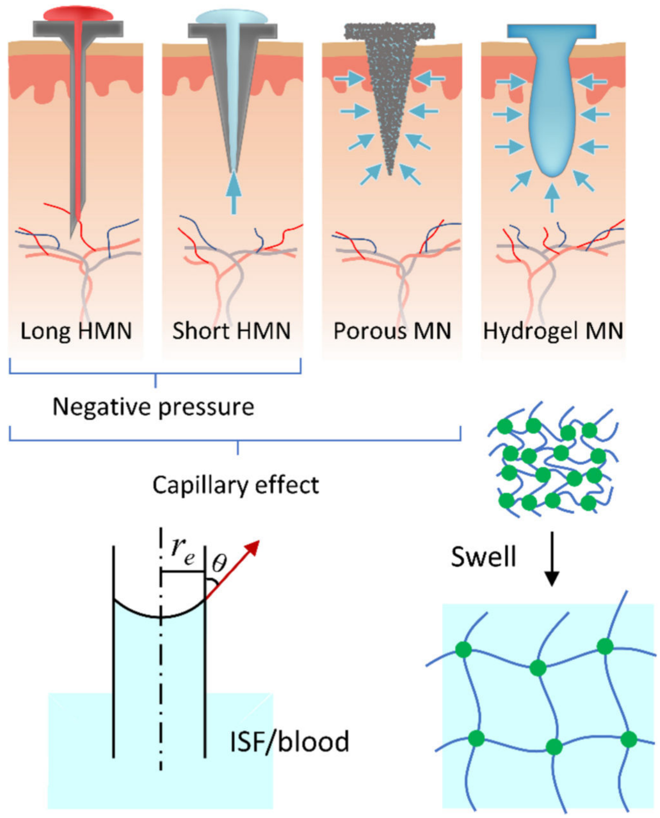

Fig. 1.

Differently shaped and structural MNs for transdermal biofluid sampling driven by negative pressure, capillarity, or swelling.

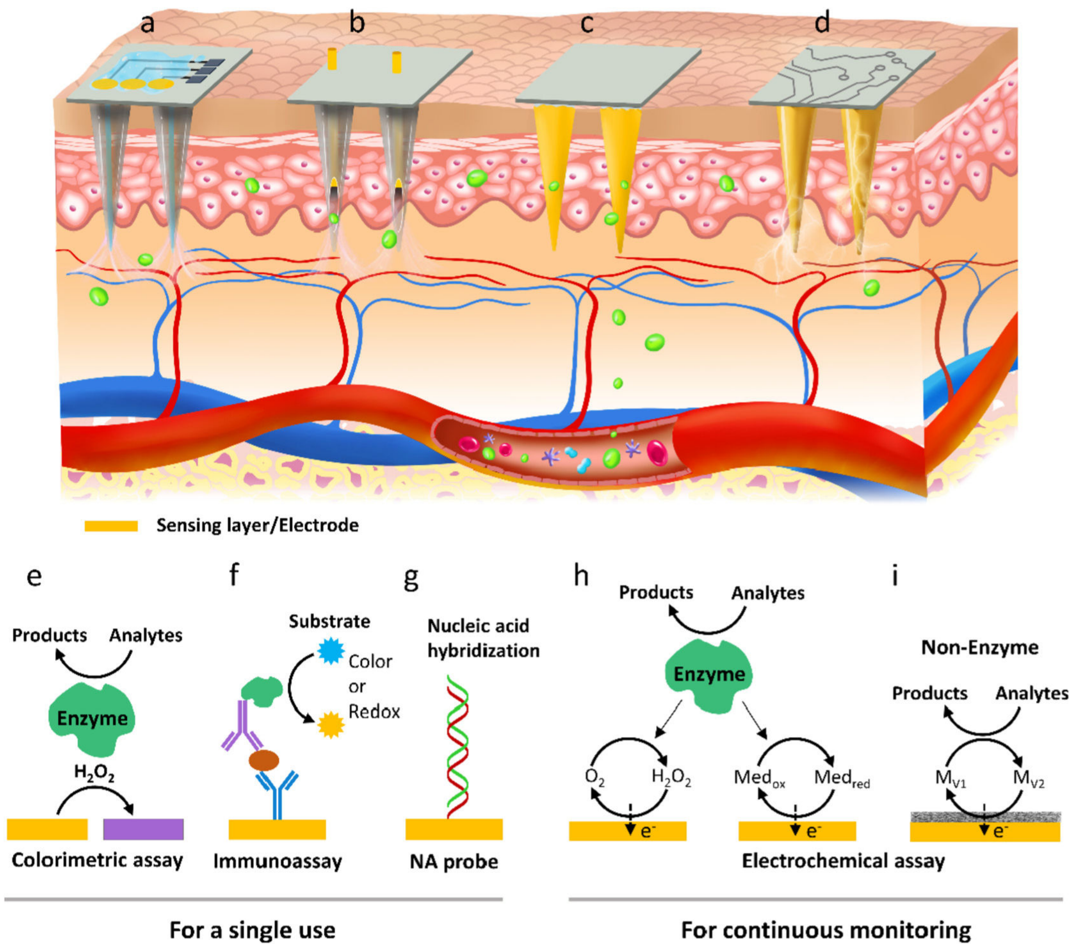

Fig. 2.

Four typical designs of MN-based sensors. (a) HMNs topped with a specific sensor, (b) electrochemical electrode incorporated HMNs, (c) surface-functionalized and (d) metalized SMNs. (e-i) Working mechanisms of different MN sensors: colorimetry, immunoassay, nucleic acid recognition, and electrochemistry.

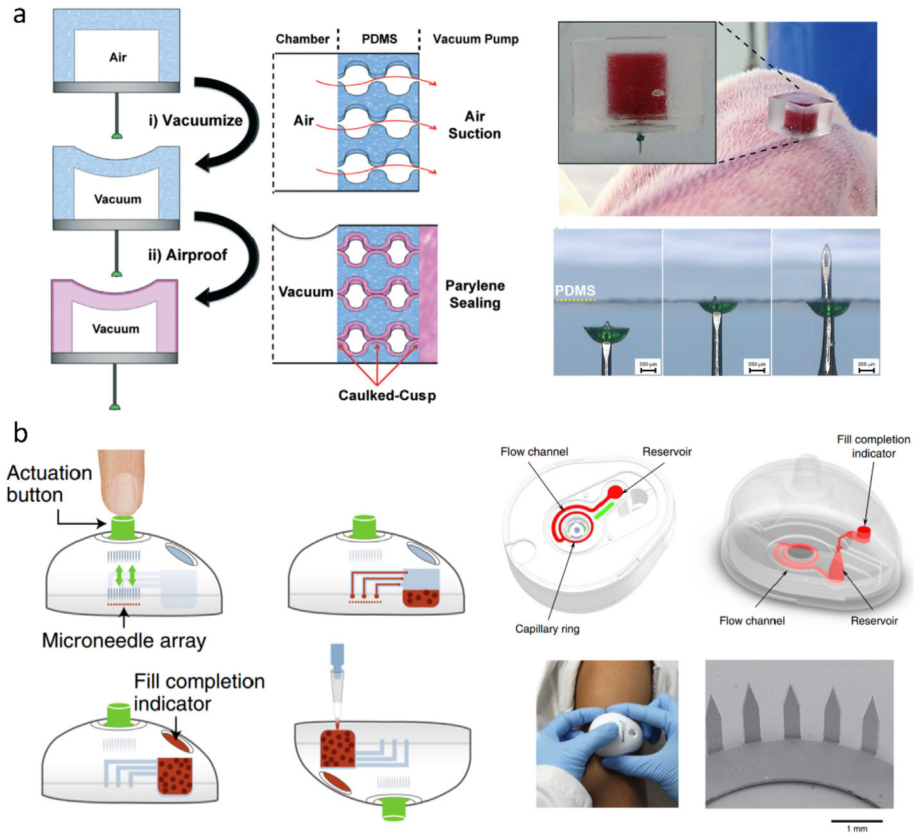

Fig. 3.

Schematics of (a) a capped HMN with a pre-vacuumized PDMS actuator [73] and (b) a SMN array-based device for blood sampling [78]. Figures reprinted with permissions from Royal Society of Chemistry and Springer Nature.

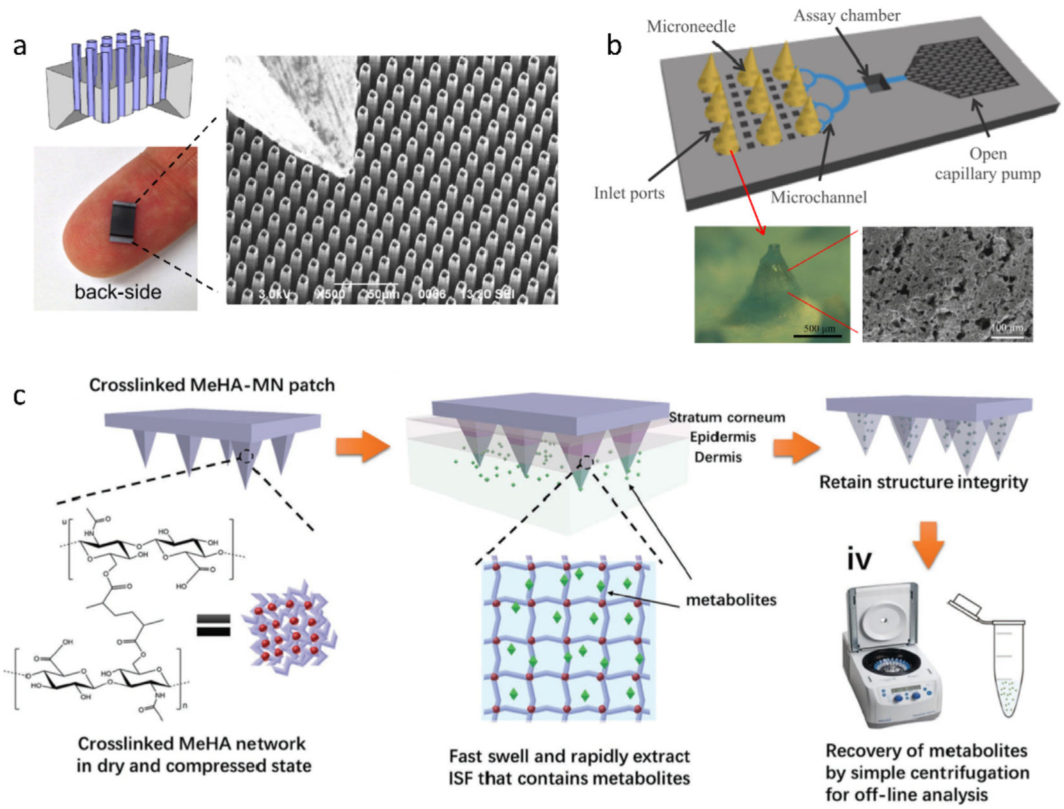

Fig. 4.

(a) Optical and SEM images of an HMN patch made of a silicon wafer. Protruding length: 100 μm; pitch: 16 μm; external diameter: 9 μm; internal diameter: 7 μm; HMN area: > 0.5 × 0.5 cm^2 [32]. (b) Schematic of PMNs-based microfluidic chip for ISF extraction and direct analysis. The optical and SEM images show the PMN made of PDMS and hyaluronic acid [33]. (c) Schematic of hydrogel MNs made of a rapidly swelling hyaluronic acid crosslinked by methacrylic anhydride for ISF extraction [34]. Figures reprinted with permissions from Elsevier, Springer Nature, and John Wiley and Sons.

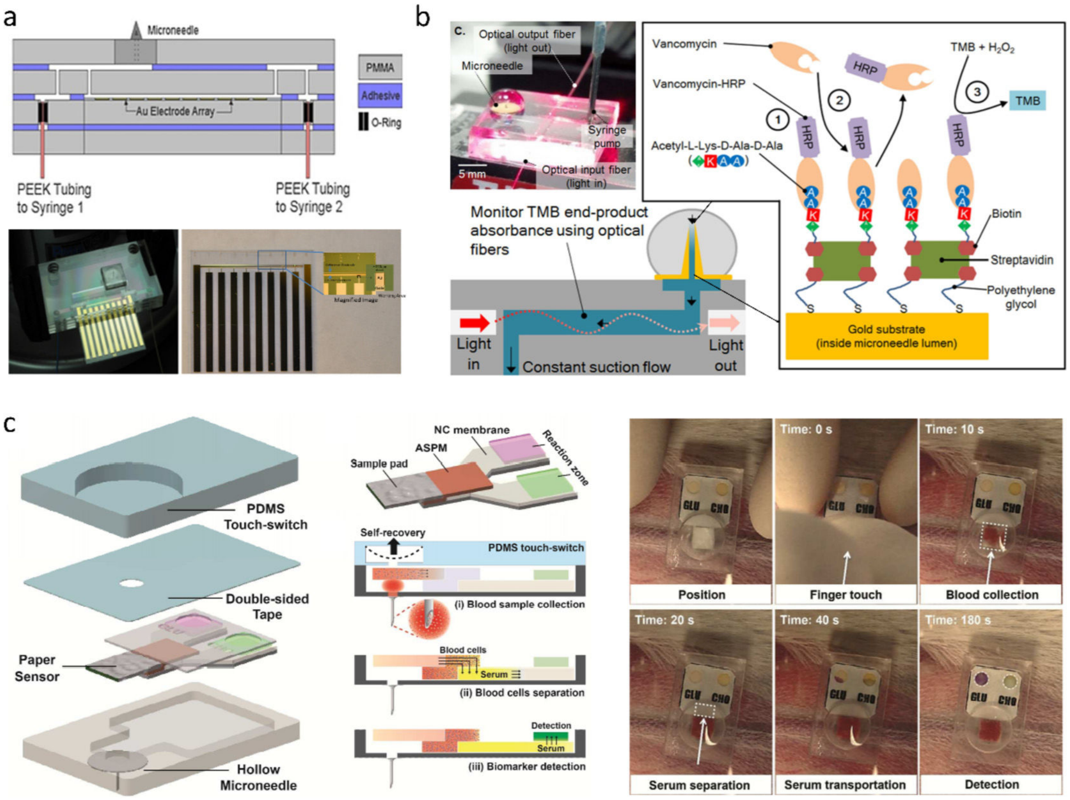

Fig. 5.

(a) HMN chip containing microfluidic channels and electrochemical electrodes [109]. (b) HMN optofluidic sensor for drug monitoring: HMN lumen is immuno-functionalized to capture vancomycin [110]. (c) HMN combined with a PDMS switch and a paper-based sensor for multi-diagnosis [89]. Figures reprinted with permissions from John Wiley and Sons and Royal Society of Chemistry.

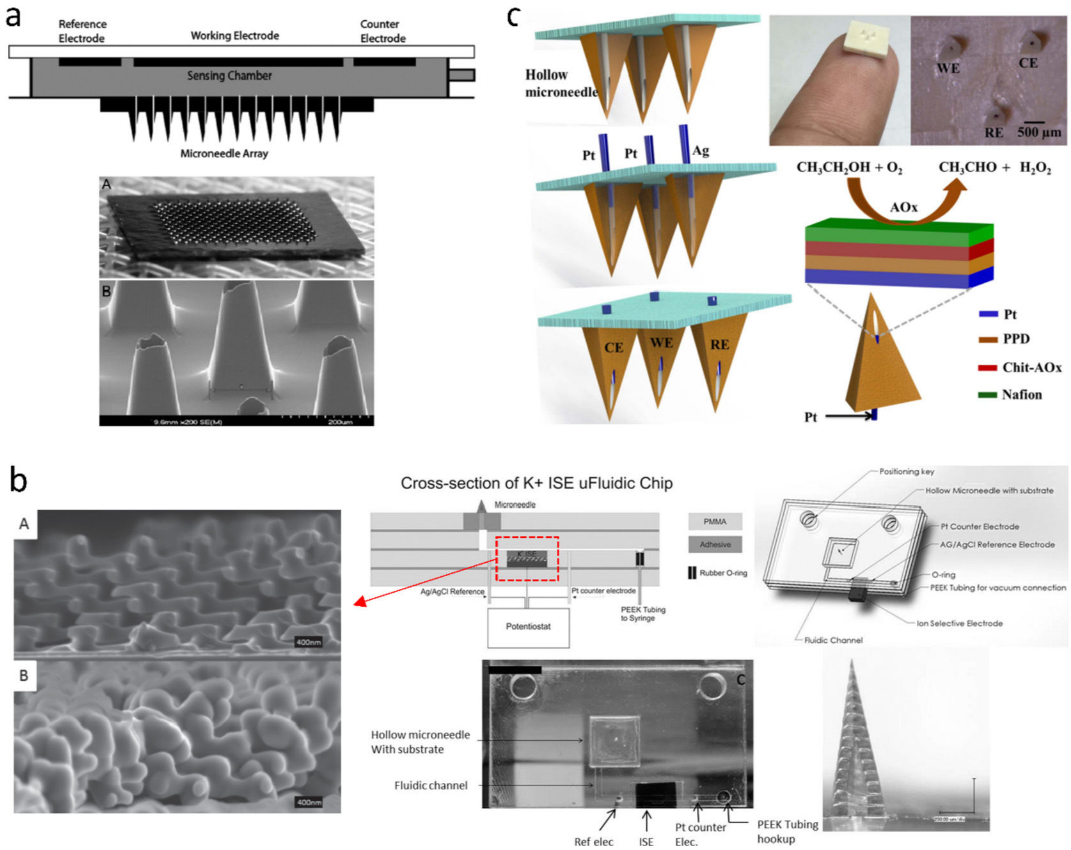

Fig. 6.
(a) Si HMN patch integrated with three electrochemical electrodes for continuous glucose monitoring [59]. (b) HMN-based microfluidic chip for potassium ions monitoring and SEM images of a 3D porous carbon-based electrode [115]. (c) Pyramidal HMN patch incorporating three electrochemical electrodes for alcohol monitoring [44]. Figures reprinted with permissions from SAGE, John Wiley and Sons, and Elsevier.

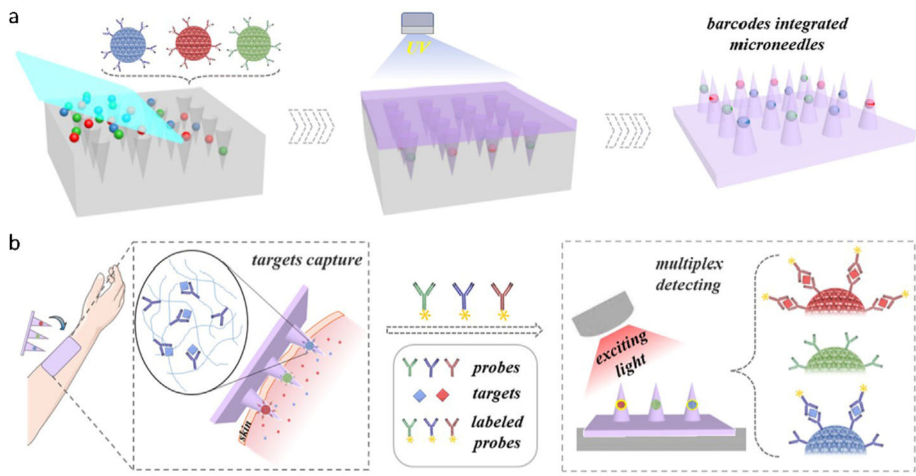

Fig. 7.
Schematic of (a) photonic crystal encoded MNs and (b) detection of multiple ISF biomarkers [127]. Figure reprinted with permission from John Wiley and Sons.

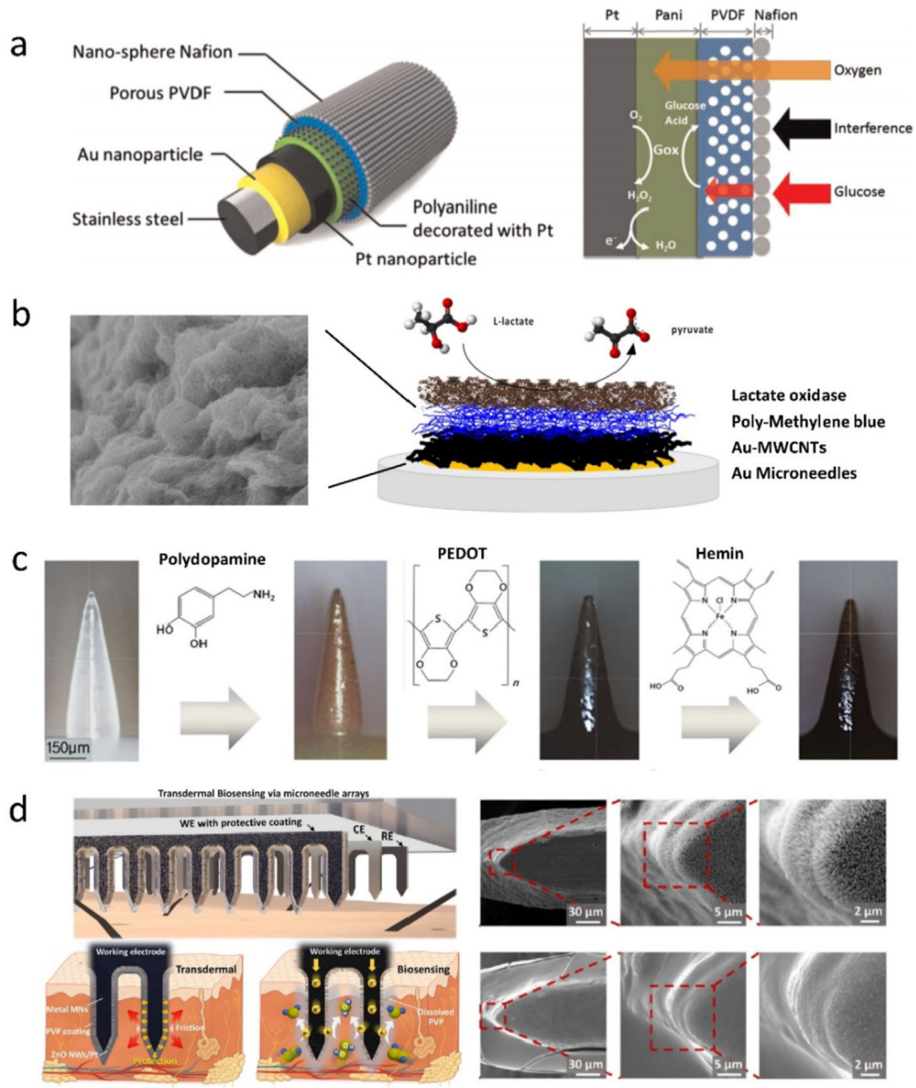

Fig. 8.

(a) Schematics of (left) functionalized stainless-steel MN (three main components: Au/Pt NPs, PVDF/Nafion layer, and glucose oxidase) and (right) glucose monitoring [133]. (b) Microscopic structure of (left) pMB-MWCNT composite and (right) SMN surface (four layers: gold, Au-MWCNTs, poly-methylene blue (pMB), and lactate oxidase) for lactate detection [62]. (c) Workflow for surface modification of a polycarprolactone (PCL) MN for real-time NO monitoring [50]. (d) Schematic of ZnO NWdecorated stainless steel MNs for H_2O_2 detection and SEM images of vertical ZnO NWs synthesized on MN surface (top) and protected by PVP (bottom) [135]. Figures reprinted with permissions from Elsevier, John Wiley and Sons, and American Chemical Society.

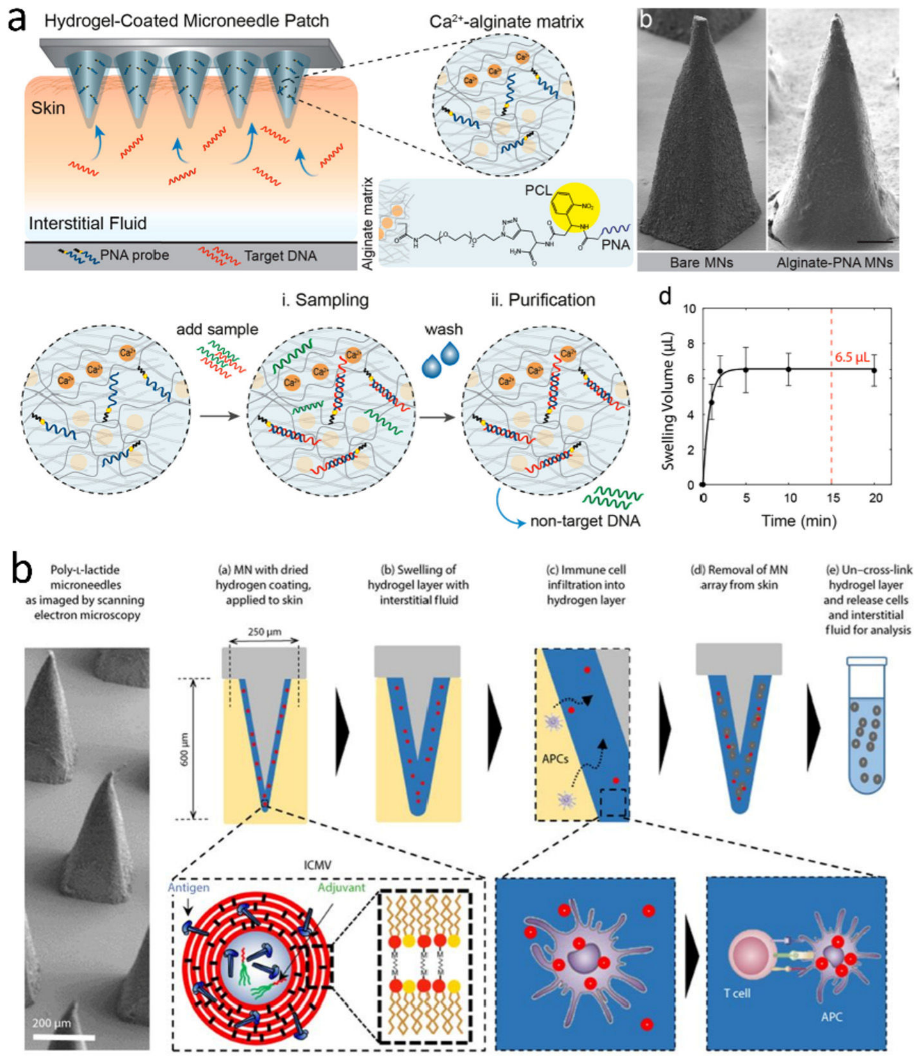

Fig. 9.

Schematics of (a) PNA-modified hydrogel/SMN for sampling NA [56] and (b) Alginate-coated SMNs for capturing T cells. Antigen-loaded nanocapsules are encased in the alginate layer [108]. Figures reprinted with permissions from American Chemical Society and The American Association for the Advancement of Science.

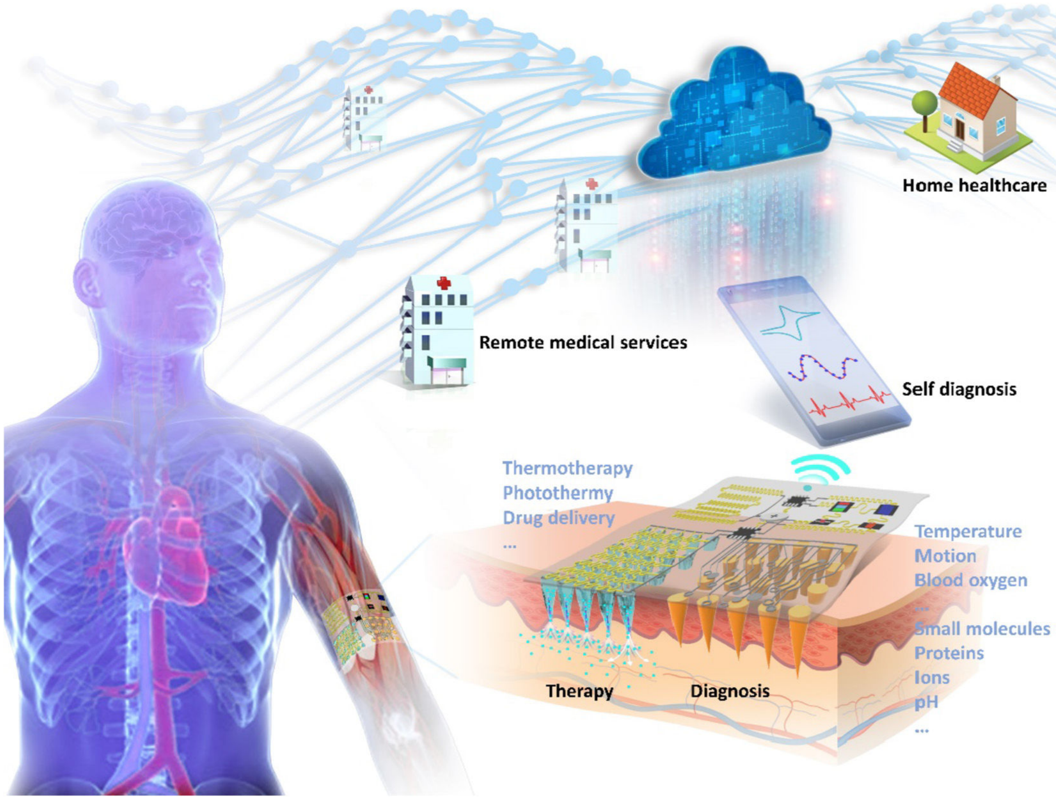

Fig. 10.
Conceptual diagram of wearable MN-based theranostic system for comprehensive personal healthcare in the near future.

Table 1

Summary of biofluid extraction using different types of MNs.

MN type	Materials	Length (μm)	Sample	Sampling volume/rate	Sampling time	Sampling method	Test subject	Ref
HMN	Si	100	ISF	1 μL s^{-1}	-	Capillary action	-	[32]
	Metal	1800	Blood	31.3 μL	4 s	Vacuum	Rabbit	[73]
		1500	Blood	31.5 μL	-	PDMS actuator	Rabbit	[74]
	Glass	1500	ISF	20 μL	1–2 h	Mechanical pressure	Human	[30]
PMN	Al_2O_3	900	Water	-	15 min	Capillary action	-	[75]
	PGMA	700	Water	-	A few seconds	Capillary action	-	[76]
		350	ISF	-	A few seconds	Capillary action	Human	[41]
	PDMS	600	PBS	1.71 nL min^{-1}	-	Compression force	-	[33]
SMN	Metal + paper	750	ISF	2 μL	1 min	Paper absorption	Wistar rat	[77]
	Metal	1000	Blood	103.5 μL	3 min	Vacuum	Human	[78]
Hydrogel MN	PMEV/MA-PEG	600	ISF	0.84 mg	1 h	Swelling	Rat	[79]
		600	ISF	-	5 min	Swelling	Human	[39]
		600	ISF	-	1 h	Swelling	Porcine	[80]
	MeHA	800	ISF	1.4 μL	1 min	Swelling	Mouse	[34]
	Alginate + PLLA	550	ISF	6.5 μL	2 min	Swelling	-	[56]

Table 2

Analytes detected by various MN sensors.

Analyte	Sensor structure	Detection method	Test subject	Detection site	Ref
Glucose	Hydrogel SMNs	Glucose assay kit	Mouse	Off device	[34]
	Metal HMN + Paper sensor	Colorimetry	Rabbit	On device	[89]
	Si HMNs + Sensor	Electrochemistry	Human	On device	[40]
	Metal SMNs + PEDOT	Electrochemistry	-	On MN	[60]
Cholesterol	Hydrogel SMNs	Cholesterol assay kit	Mouse	Off device	[34]
	Metal HMNs + Paper sensor	Colorimetry	Rabbit	On device	[89]
Glutamate	Polymer HMNs + SMNs	Electrochemistry	-	On MN	[58]
Lactate	Polymer HMNs + Carbon paste	Electrochemistry	-	On MN	[42,43]
	Polymer SMNs + MWCNTs	Electrochemistry	-	On MN	[62]
Influenza IgG	Si SMNs + Antigen	ELISA	Mouse/Swine	On MN	[49,121,128]
NS1 Protein	Si MNs + Antibody	ELISA	Mouse	On MN	[119]
Pf HRP2	Si MNs + Antibody	ELISA	Mouse	On MN	[122]
IL-lα, IL-6, TNF-α	Polymer SMNs + Antibodies	ELISA-blotting method	Mouse skin, *Ex vivo*	On MN	[126]
	Polymer SMNs + PhC barcodes	ELISA + Spectra	Sepsis mouse	On MN	[127]
Myoglobin; Troponin	Polymer HMNs + Immunoelectrodes	Electrochemical immunoassay	-	On MN	[109]
Ascorbic acid	Polymer HMNs + Carbon fibers	Electrochemistry	-	On MN	[66]
K^+	Polymer HMNs + ISE	Electrochemistry	-	On device	[115]
	Metal SMN + ISE	Electrochemistry	Chicken/porcine skin, *Ex vivo*	On MN	[170]
NO	Polymer SMNs + Hemin + Endomicroscopy	Electrochemistry	Melanoma mouse	On MN	[50]
	Metal SMN + FGPC	Electrochemistry	Rat	On MN	[142]
pH	Metal SMN + BDD	Electrochemistry	Mouse stomach, *Ex vivo*	On MN	[145]
	Metal SMN + ZnO	Electrochemistry	Mouse	On MN	[67]
	Polymer SMN + IrOx	Electrochemistry	Rat heart, *Ex vivo*	On MN	[130]
H_2O_2	Metal SMN + Pt/rGO	Electrochemistry	Mouse	On MN	[[149]
Alcohol	Polymer HMNs + Electrodes	Electrochemistry	Mouse skin, *Ex vivo*	On device	[44]
Vancomycin	Metal HMNs + Peptide	ELISA-optofluidic detection	-	On device	[110]
β-Lactam Antibiotic	Polymer SMNs + g-lactamase	Electrochemistry	-	On MN	[51]
Organophosphate	Polymer HMNs + Carbon paste	Electrochemistry	Mouse stomach, *Ex vivo*	On device	[44, 46]

Analyte	Sensor structure	Detection method	Test subject	Detection site	Ref
Levodopa			Porcine skin, *Ex vivo*		[48]
Tyrosinase					[47]
DNA-210	Polymer SMNs + PNA oligomers	PNA hybridization	Human skin, *Ex vivo*	On MN	[56]
T cell	Polymer SMNs + Antigen Nano capsules	Immune response	Human skin, *Ex vivo*	Off device	[108]